Phosphatidylinositol 4,5-bisphosphate (PIP_2) regulates KCNQ3 K^+ channels by interacting with four cytoplasmic channel domains

Received for publication, August 15, 2018, and in revised form, October 12, 2018 Published, Papers in Press, October 22, 2018, DOI 10.1074/jbc.RA118.005401

Frank S. Choveau[‡], Victor De la Rosa[‡], Sonya M. Bierbower[‡1], Ciria C. Hernandez[§¶2], and Mark S. Shapiro[‡3]

From the [‡]Department of Cell and Integrative Physiology, University of Texas Health San Antonio, San Antonio, Texas 78229, the [§]Department of Neurology, Vanderbilt University Medical Center, Nashville, Tennessee 37232, and the [¶]Life Sciences Institute, University of Michigan, Ann Arbor, Michigan 48109

Edited by Mike Shipston

Phosphatidylinositol 4,5-bisphosphate (PIP_2) in the plasma membrane regulates the function of many ion channels, including M-type (potassium voltage-gated channel subfamily Q member (KCNQ), K_v7) K^+ channels; however, the molecular mechanisms involved remain unclear. To this end, we here focused on the KCNQ3 subtype that has the highest apparent affinity for PIP_2 and performed extensive mutagenesis in regions suggested to be involved in PIP_2 interactions among the KCNQ family. Using perforated patch-clamp recordings of heterologously transfected tissue culture cells, total internal reflection fluorescence microscopy, and the zebrafish (*Danio rerio*) voltage-sensitive phosphatase to deplete PIP_2 as a probe, we found that PIP_2 regulates KCNQ3 channels through four different domains: 1) the A–B helix linker that we previously identified as important for both KCNQ2 and KCNQ3, 2) the junction between S6 and the A helix, 3) the S2–S3 linker, and 4) the S4–S5 linker. We also found that the apparent strength of PIP_2 interactions within any of these domains was not coupled to the voltage dependence of channel activation. Extensive homology modeling and docking simulations with the WT or mutant KCNQ3 channels and PIP_2 were consistent with the experimental data. Our results indicate that PIP_2 modulates KCNQ3 channel function by interacting synergistically with a minimum of four cytoplasmic domains.

Voltage-gated K^+ (K_v)[4] channels play critical roles in the function of various tissues, including brain, heart, and epithelia (1). Among K_v channels, KCNQ1–5 ($K_v7.1$–7.5) channels are regulated by several intracellular signaling molecules, including phosphatidylinositol 4,5-bisphosphate (PIP_2), which is present in the inner leaflet of the cell plasma membrane at only modest abundance. For some time, it has been known that interactions with PIP_2 regulate M-channel activity (2–7). However, the answers to several key questions remain elusive: How and where does PIP_2 regulate KCNQ channels, and are those mechanisms disparate between KCNQ1-containing channels and the others, or do they generalize among KCNQ1–5? To understand the molecular mechanisms by which PIP_2 regulates KCNQ channels, it is necessary to identify the site(s) of PIP_2 interaction. K_v channels are tetramers of subunits containing six transmembrane domains (S1–S6). The earliest study suggested that PIP_2 interacts with the junction between S6 and the first C-terminal "A helix" (which we call the S6Jx domain) of KCNQ2; thus, replacement of the histidine at position 328 in the S6Jx of KCNQ2 (His^{367} in KCNQ3; Fig. 1*A*) by a cysteine reduced the sensitivity of the channel to PIP_2 (4). We identified a "cationic cluster" (Lys^{452}, Arg^{459}, and Arg^{461} in KCNQ2) in the linker between the A and B helices (A–B linker) of KCNQ2 and KCNQ3, which were suggested to form electrostatic bonds with the phosphate headgroups of PIP_2 molecules (8). Expanding on those findings, Tinker and co-workers (9) localized a cluster of basic residues (Lys^{354}, Lys^{358}, Arg^{360}, and Lys^{362}) in the S6Jx of KCNQ1 channels. In KCNQ3, the analogous Lys^{358}, Gln^{362}, Arg^{364}, and Lys^{366} residues (Fig. 1*A*) were suggested to interact with PIP_2. More recent work has suggested two additional domains that interact with PIP_2 and regulate gating, the linker between transmembrane helices S2 and S3 (S2–S3 linker) and between the S4 and S5 helices (S4–S5 linker), domains in KCNQ1 channels whose interactions with PIP_2 were suggested moreover to be important for coupling between the voltage sensor and the gate (10). Lastly, a recent study based heavily on molecular dynamics simulations suggested state-dependent interactions between PIP_2 and the S2–S3 and S4–S5 linkers of KCNQ2 channels that were weakly coupled to the voltage dependence of activation (11).

This work was supported by National Institutes of Health Grants R01 NS150305, R01 NS094461, and R56 NS153503 (to M. S. S.). The authors declare that they have no conflicts of interest with the contents of this article. The content is solely the responsibility of the authors and does not necessarily represent the official views of the National Institutes of Health.

This article contains Figs. S1–S3.

[1] Present address: Dept. of Biology, College of Science and Health, William Paterson University, Wayne, NJ 07470.

[2] To whom correspondence may be addressed: Life Sciences Institute, University of Michigan, Rm. 6115, 210 Washtenaw Ave., Ann Arbor, MI 48109-2216. Tel.: 734-615-1867; Fax: 734-647-9702; E-mail: ciria@umich.edu.

[3] To whom correspondence may be addressed: Dept. of Cell and Integrative Physiology, University of Texas Health San Antonio, South Texas Research Facility, MC 8253, 8403 Floyd Curl Dr., San Antonio, TX 78229. Tel.: 210-562-4092; Fax: 210-562-4060; E-mail: shapirom@uthscsa.edu.

[4] The abbreviations used are: K_v, voltage-gated K^+; K_{ir}, inward rectifier K^+; KCNQ, potassium voltage-gated channel subfamily Q member; PIP_2, phosphatidylinositol 4,5-bisphosphate; VSP, voltage-dependent phosphatase; PI(4)P, phosphatidylinositol 4-phosphate; M_1R, muscarinic acetylcholine receptor, type 1; PI(4)P-5, phosphatidylinositol-4-phosphate 5-kinase; Dr-VSP, *Danio rerio* VSP; pF, picofarads; CaM, calmodulin; TIRF, total internal reflection fluorescence; VSD, voltage sensor domain; PD, pore domain; CHO, Chinese hamster ovary; EGFP, enhanced green fluorescent protein; EYFP, enhanced yellow fluorescent protein; PDB, Protein Data Bank.

Lending support for a generalized structural interaction between PIP_2 and the region just distal to the final transmembrane helix of K^+ channels is the crystal structure of PIP_2 bound to the $K_{ir}2.2$ channel (12), which shows a PIP_2 molecule interacting with residues not only in the proximal C terminus as it emerges from the lipid bilayer, but also residues at the distal end of the M2 helix. Thus, it behooved us to more systematically examine all of these regions of a KCNQ channel most amenable to study via a voltage-dependent phosphatase (VSP), which can dephosphorylate nearly all of the PIP_2 in the plasma membrane within about 500 ms (13). This method has been exploited to examine the PIP_2 sensitivity of KCNQ (14, 15) and TRP (16) channels, among others. Most significantly, unlike reducing PIP_2 abundance by stimulating G_q– and phospholipase C–coupled receptors, which could also produce inositol triphosphate, Ca^{2+} rises, activate protein kinase C and induce other downstream signals, activation of VSP only dephosphorylates PIP_2 to PI(4)P, a singly phosphorylated lipid that does not allow activation of M channels (17, 18).

The Hille group (14) studied KCNQ2/3 heteromers and found the time constant of dephosphorylation of available PIP_2 in the membrane of a tissue culture cell to be ~250 ms; in that work, while not quantifying the k_{on} or k_{off} of PIP_2, they found a "dwell time" of ~10 ms to be consistent with the modeling of their data, most likely due to the low affinity of KCNQ2 subunits that determine whether KCNQ2/3 channels are open or closed due to PIP_2 interactions. Hence, mutations that decrease their apparent affinity of PIP_2, resulting in "dwell times" necessarily shorter than 10 ms in KCNQ2-containing channels cannot possibly be meaningfully quantified during the decay of the current during the depolarization step to a very positive potential that activates *Danio rerio* VSP (Dr-VSP), because any shorter k_{off} would be wholly confounded by the time required for PIP_2 dephosphorylation. In such a case, only an altered rate of recovery of the current, reflecting an altered k_{on}, could be meaningful. Thus, such relatively low PIP_2 apparent affinity channels are unsuitable for this approach. For these reasons, we chose the KCNQ3 homomer as our test channel, due to its extremely high apparent affinity for PIP_2, as manifested by its saturating open probability near unity at saturating voltages and its maximal depression by M_1 receptor stimulation of only ~40% (5, 19) *versus* <0.3 and 90%, respectively, for all other KCNQ isoforms and compositions. Our assumption was that that this channel would be amenable to such analysis using the VSP approach and that high structural and mechanistic similarity with the other KCNQ subtypes should make our data generalizable among this K^+ channel family. In some experiments, we used the alternative assay of quantifying the extent of depression of the current by stimulation of muscarinic M_1 acetylcholine receptors (M_1Rs) co-expressed with the channels (see below).

In our patch-clamp experiments, we used the well-expressing KCNQ3-A315T (KCNQ3T) channel as a baseline, an inner-pore mutant that increases whole-cell current amplitudes by >10-fold (20, 21, 73), without changing the open probability of the channels or their apparent PIP_2 affinity (19). We probed the effects of charge neutralizations in the S2–S3 linker, the S4–S5 linker, the S6Jx domain, and the A–B helix linker on changes in the apparent PIP_2 affinity of the channels as well as their voltage dependence of activation. In addition, homology modeling and PIP_2-docking simulations were performed to seek a structural framework for our experimental results. We find that all of the regions tested are involved, complementing the PIP_2-binding "cationic cluster" described previously in the A–B helix linker of KCNQ2 and KCNQ3 (8). Whereas the four domains identified here for KCNQ3 as interacting with PIP_2 are conserved with KCNQ1, and likely KCNQ2, mutations that lowered the apparent affinity of the channels for PIP_2 were not correlated with alterations in voltage dependence.

Results

We chose Dr-VSP because it activates at +40 mV, well positive to the saturating voltage for all KCNQ channels. Upon activation of Dr-VSP by depolarization to +120 mV, which dephosphorylates PIP_2 into PI(4)P, quantification of the rate of decay of the current provides an estimate of changes in k_{off} of PIP_2 from the channels due to mutations. We realize that this is an approximation, due to the confound of the known rate of Dr-VSP dephosphorylation of PIP_2 by Dr-VSP at that voltage (τ ~250 ms). However, the deconvolution of those rates is beyond the scope of this paper; moreover, we would need information on the allosteric influence of the binding of one PIP_2 molecule to one subunit on its affinity with another and the precise number of PIP_2 molecules required for the opening of KCNQ3 homomers, and both sets of data are lacking at this time. Upon the step back to +30 mV, changes in k_{on} of PIP_2 due to mutations were estimated by the rate of recovery of the current. We again realize that this estimate is an approximation due to the confound of the known rate of PI(4)P-5 kinase (τ ~10 s) (14). Again, an even more sophisticated deconvolution would be extremely difficult without more information, which is also not presently available.

Besides the measurements described above, we also compared the amplitude of tonic whole-cell currents between cells transfected with KCNQ3T and mutant KCNQ3T channels and the voltage dependence of activation. The first measurement is based on the correlation between the tonic open probability at the single-channel level, macroscopic current amplitudes, and PIP_2 apparent affinity observed for KCNQ2, KCNQ2/3, KCNQ3, and KCNQ4 channels (5, 19) and other PIP_2-regulated channels (*e.g.* GIRK channels) as well (6, 22). The voltage dependence of activation is important because whether PIP_2-mediated depression of KCNQ1-containing channels is accompanied by altered voltage dependence is still open to debate (3, 10), and PIP_2-mediated modulation of KCNQ2/3 channels does not change the voltage dependence of activation (23–25). Whereas the A–B helix linker "cationic" cluster domain identified in PIP_2 interactions with KCNQ2 and KCNQ3 in our previous work (19) is not conserved in KCNQ1, the S6Jx, S4–S5 linker, and S2–S3 linker PIP_2-interaction domains are conserved, which for KCNQ1 were suggested to form a network of PIP_2-interacting domains that are involved in voltage sensor/gate coupling (10). We were therefore keen to investigate these issues for the case of KCNQ3, which is found primarily in neurons, as opposed to cardiomyocytes or epithelia. With the parameters and assumptions given, we can now present the data.

Interactions of PIP_2 with the S2–S3 and the S4–S5 linkers in KCNQ3

Several recent studies have suggested a potential role of the S2–S3 and the S4–S5 linkers in PIP_2–KCNQ channel interactions (10, 11, 26, 27). Because these sites are most novel in terms of PIP_2 interactions suggested for KCNQ2–5 channels, we begin here. For KCNQ1, the interactions with the S2–S3 linker involve Arg^{190} and Arg^{195}, and for the S4–S5 linker, they involve Arg^{243}, His^{258}, and Arg^{259}. The sequence alignment of the S2–S3 and the S4–S5 linkers among KCNQ1–5 channels (Fig. 1*A* and Fig. S3*E*) indicates the Arg^{190}, Arg^{195}, and His^{258} residues to be conserved. The perforated patch variant of whole-cell recording was performed to maintain the intracellular milieu and prevent "run-down" of PIP_2 abundance. We tested the effect of charge-neutralizing mutations at the analogous positions, Arg^{190} and Arg^{195}, in the S2–S3 linker and His^{257} (corresponding to His^{258} in KCNQ1) in the S4–S5 linker of KCNQ3T (Figs. 1 (*A–C*) and 2). In the S2–S3 linker, the R190Q mutation, but not R195Q, decreased current densities from 197 ± 6 to 66 ± 12 pA/pF (Fig. 2 (*A* and *B*) and Table 1). Using the Dr-VSP assay, we found the rate of current decay upon depolarization that turns on Dr-VSP (τ_{decay}) for the R190Q mutant (0.35 ± 0.11 s) to be much faster than for KCNQ3T (0.94 ± 0.13 s) (Fig. 2 (*D* and *E*)); however, the rates of recovery of the current ($\tau_{recovery}$) were not significantly different (7.5 ± 1.7 s *versus* 9.6 ± 1.6 s for KCNQ3T and R190Q, respectively). The same result was obtained from the analogous mutant R190A (τ_{decay} = 0.35 ± 2 s, $\tau_{recovery}$ = 7.5 ± 1.8 s). Neither response was altered by the R195Q mutation. Either Arg^{190} influences K_{off} for PIP_2, but not k_{on}, or our assay is not sensitive enough to detect changes in both rates accurately. As an alternative assay, we thus turned to the classic M_1R-dependent depression of the current in cells co-expressing M_1 muscarinic receptors and KCNQ3T mutants. Because maximal M_1R stimulation in tissue culture cells leads to about an 80% decrease in PIP_2 abundance, rather than to near zero when VSPs are activated (14), the maximal depression of KCNQ3 currents is only ~30–40%, because enough PIP_2 molecules remain in the membrane to keep most KCNQ3 channels PIP_2-bound (19, 24). Thus, for such high PIP_2 apparent affinity channels, a change in that affinity is manifested most in the fractional suppression of the current, not a shift of the dose–response relation of [agonist] *versus* current suppression (Fig. S1*F*). In these experiments, we decided to use mutants in which the arginines at positions 190 and 195 were mutated to alanines instead of the highly hydrophilic and bulky glutamines, which can interact with PIP_2 via several types of H^+ bonds, to avoid any such confounding effects. Consistent with previous work, we found the KCNQ3T current to be suppressed by a supramaximal concentration (10 μM) of the receptor agonist, oxotremorine methiodide, by only 29.5 ± 5.5%, and for cells expressing KCNQ3T-R195A, the maximal inhibition was only 24.9 ± 5.8%. However, for KCNQ3T-R190A, the maximal inhibition was 63 ± 13%, indicating that the R190A mutation reduces PIP_2 affinity, consistent with the Dr-VSP assay (Fig. 2*G* and Fig. S1). Neither the R190Q/A nor the R195Q/A mutations affected the voltage dependence of activation (Fig. 2*C*), suggesting that the apparent affinity of PIP_2 for this site is unrelated to voltage dependence.

We found the H257N mutation in the S4–S5 linker (Figs. 1 (*B* and *C*) and 2) to result in strongly reduced current densities, from 197 ± 6 to 30 ± 3 pA/pF. The rate of current decay after Dr-VSP activation was much faster than KCNQ3T (0.58 ± 0.14 s), and the rate of recovery was slightly slower (11.0 ± 1.4 s), although it was not suitable for analysis in most of the cells recorded, probably due to the astounding shift in the voltage dependence of activation from −34.0 ± 1.9 mV for KCNQ3T to 2.5 ± 2.8 mV for H257N. Thus, we turned again to quantifying the result of M_1R stimulation. For cells co-transfected with M_1Rs and the KCNQ3T-H257N mutant, the maximal inhibition was 81.6 ± 7.9% (Fig. 2*G* and Fig. S1). Together, these results indicate that the H257N mutation reduces the apparent PIP_2 affinity of the channels.

Because the R243H mutation in the S4–S5 linker was shown to reduce the apparent affinity of KCNQ1 for PIP_2 (26) and Arg^{243} is conserved in other KCNQ channels (Arg^{242} in KCNQ3) (Fig. 1*A*), we also tested the effect of the R242A mutation in KCNQ3T channels (Fig. 2). This mutant resulted in reduced current densities (146 ± 16 pA/pF) and slowed current recovery (14.2 ± 1.7 s) in the VSP assay; however, the rate of decay upon turn-on of Dr-VSP was not significantly affected. M_1R stimulation inhibited the current by 64.8 ± 9.2%, 2-fold greater than for KCNQ3T (Fig. 2*G* and Fig. S1). These results are consistent with a role of Arg^{242} in PIP_2 interactions. This mutation resulted also in a pronounced shift of the voltage dependence of activation toward more positive potentials ($V_{½}$ = −4.0 ± 3.2 mV) (Fig. 2*C*). The adjacent mutation R243A was also tested. This mutant displayed reduced current densities as well (56 ± 16 pA/pF), a faster rate of current decay upon Dr-VSP turn-on (0.59 ± 0.19 s), slowed recovery after Dr-VSP turn-off (13.1 ± 1.8 s), and a significantly increased M_1R-dependent inhibition of 42 ± 5.5%. Surprisingly, the voltage dependence of activation for this mutant, which is adjacent to R242A, was not altered ($V_{½}$ = −31 ± 4.7 mV). When both arginines were mutated to alanines, the whole-cell current densities were reduced (65 ± 11 pA/pF), as for the R243A single mutant. The rate of current decay and recovery after Dr-VSP turn-on or turn-off were significantly affected (0.45 ± 0.11 and 15 ± 1.7 s) to a greater extent than for either of the single mutations. The voltage dependence of activation of the double mutant displayed the same positive shift as for the R242A single mutant ($V_{½}$ = −0.2 ± 2.9 mV). Last, the M_1R-mediated inhibition of the double mutant was very high (91.6 ± 2.7%; Fig. 2*G*). These results are consistent with an interaction of the KCNQ3 S4–S5 linker with PIP_2, which again seems not to be coupled to the voltage dependence of activation of the channels. Clearly, however, the S4–S5 linker of KCNQ3 itself is coupled to channel voltage dependence or to the coupling mechanism, just not in a way that involves PIP_2. These data are summarized in Table 1.

Interactions of PIP_2 with the S6Jx domain in KCNQ3 channels

Three basic residues (Lys^{354}, Arg^{360}, and Lys^{362}) in the S6Jx of KCNQ1, which are conserved in KCNQ3 (Lys^{358}, Arg^{364}, and Lys^{366}) (Fig. 1*A* and Fig. S3*E*), have been found to play a role in

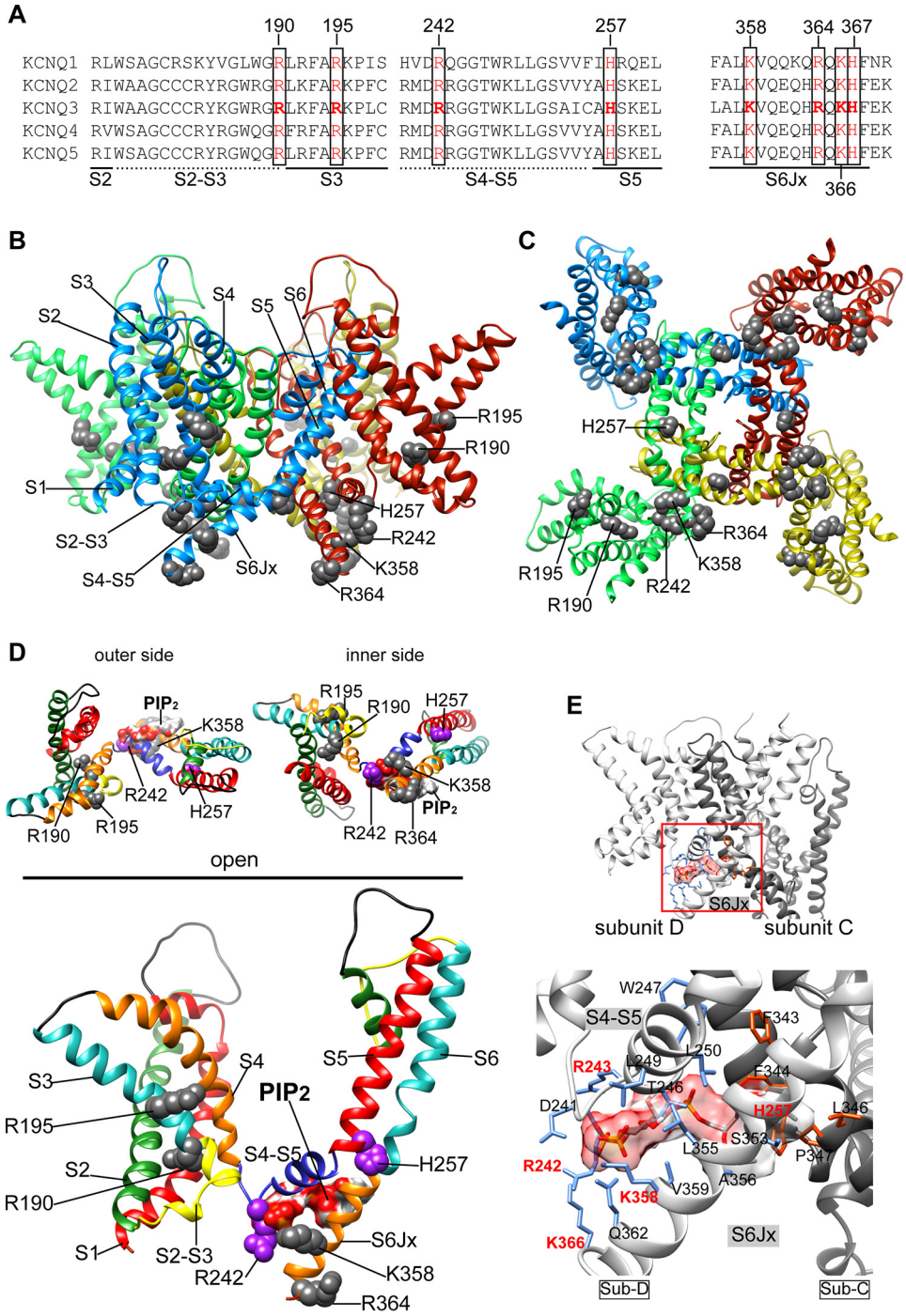

Figure 1. Location of the site(s) of PIP_2 action on KCNQ3 channels. *A*, sequence alignments of human KCNQ channels of the putative PIP_2-interaction domains studied in this work. The residues *highlighted* in *red* are conserved basic residues across all KCNQ channels. Structural domains where the putative PIP_2-interacting residues are located are indicated *below* the alignments as *solid lines* (α-helices) and *noncontinuous lines* (linkers). *B* and *C*, three-dimensional structural models of the open conformation of the KCNQ3 channel in a *ribbon representation*, *colored* by subunits as viewed from the membrane plane (*B*) and the intracellular side (*C*). Conserved basic residues Arg^{190}, Arg^{195}, Arg^{242}, His^{257}, Lys^{358}, and Arg^{364} tested in this study by mutagenesis are shown in *gray* and mapped onto the channel. *D*, *ribbon representations* of the arrangement of the VSD–PD interface of a structural subunit model viewed from the outer and inner side (*top panels*), and membrane plane (*bottom panels*). The secondary structure of the channels is *colored* according to structural domain, as indicated. Side chains of basic residues involved in PIP_2 interactions are shown in *color*, according to structural domain (*gray* for the S2–S3 linker and S6Jx and *purple* for the S4–S5 linker). The PIP_2 molecule is shown in a *molecular surface representation* within the docking cavity. *E*, expanded view of the most favorable binding model of PIP_2 in the open conformation. *Panels* show two neighboring subunits (*Sub*) forming the VSD–PD interface (Sub-C and Sub-D). The docking site *enclosed* in a *red box* was enlarged for clarity. Shown in a *stick representation* are the residues forming hydrogen bonds and electrostatic interactions within the interaction site. Residues in *blue* from the Sub-D enclose the phosphate groups of PIP_2, and residues in *orange* from the Sub-C enclose the acyl tail of the PIP_2 between Sub-C and Sub-D at the S6Jx. The following are the favorable interactions (*labeled* in *red*) predicted to be in the PIP_2-docking network ($<$6.0 Å, kJ/mol): $Arg^{242} = -12.26$, $Arg^{243} = -4.60$, $His^{257} = -1.10$, $Lys^{358} = -4.28$, $Lys^{366} = -5.74$. Hydrogen bonds are not shown.

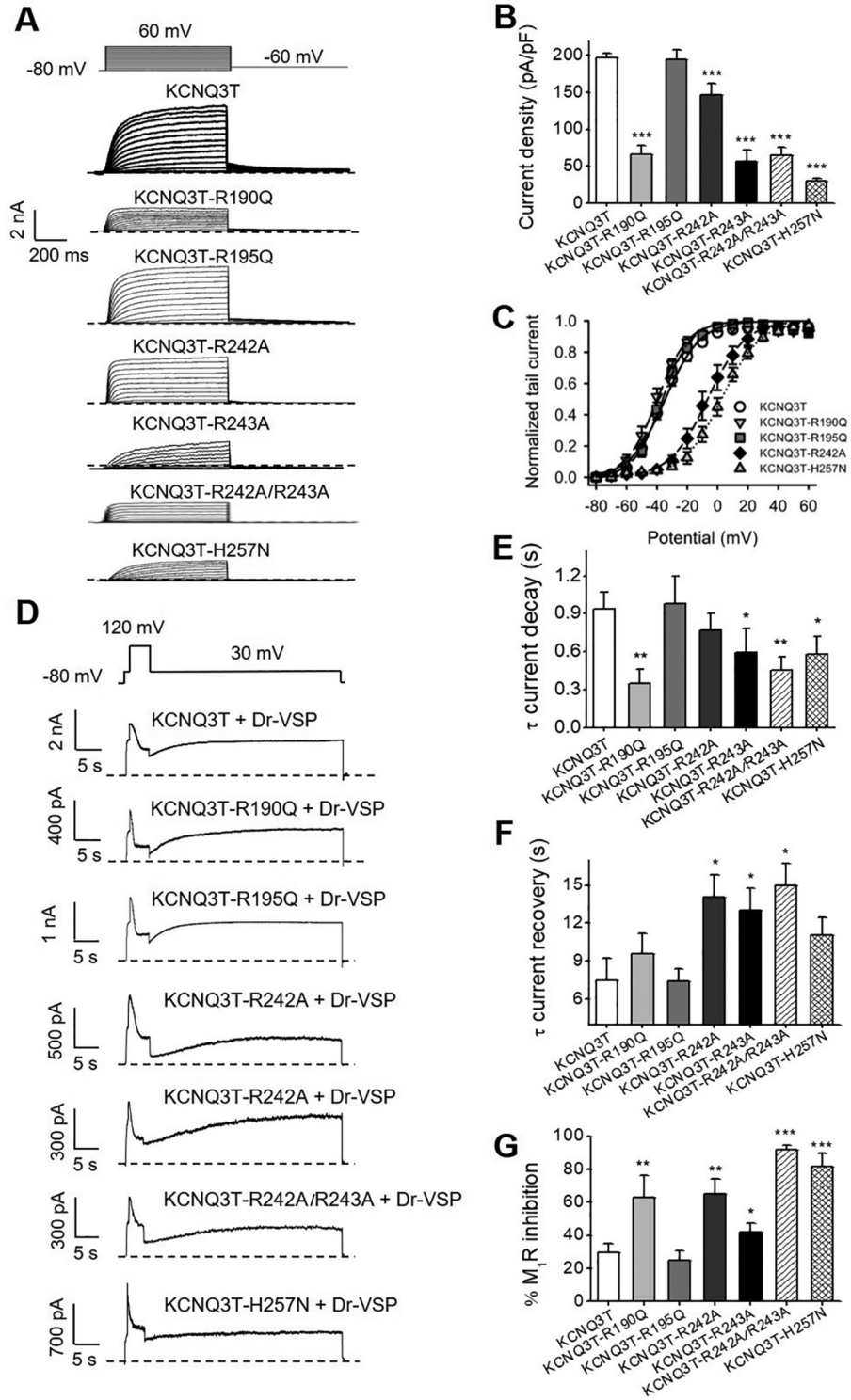

Figure 2. Effects of charge-neutralizing mutations located in the S2–S3 and S4–S5 linkers on KCNQ3T channels. *A*, representative perforated patch-clamp recordings from CHO cells transfected with KCNQ3T or the indicated mutant channels. *B*, *bars* show summarized current densities at 60 mV for the indicated channels ($n = 6–19$). *C*, voltage dependence of activation of the tail currents at −60 mV, plotted as a function of test potential ($n = 5–19$). *D*, representative perforated patch-clamp recordings from CHO cells co-transfected with Dr-VSP and KCNQ3T or the indicated mutant channels. *E*, bars summarize time constant values from single exponential fits to current decay during Dr-VSP activation ($n = 5–10$). *F*, *bars* summarize time constants of single exponential fits to current recovery after Dr-VSP turn-off ($n = 5–11$). *G*, *bars* summarize fractional inhibition after M_1R stimulation for the indicated mutant channels ($n = 3–7$). *, $p < 0.05$; **, $p < 0.01$; ***, $p < 0.001$. *Error bars*, S.E.

PIP_2 interactions (28). In addition, Telezhkin *et al.* (18) found the R325A mutation in KCNQ2, homologous to Arg^{360} in KCNQ1 and Arg^{364} in KCNQ3, to decrease the apparent affinity of the channel for DiC8-PIP_2, and early work implicated a role of His^{328} in KCNQ2, homologous to His^{367} in KCNQ3 (4). Because the Lys^{358}, Arg^{364}, Lys^{366}, and His^{367} residues in the S6Jx domain are conserved among KCNQ channels (Fig. 1*A*), we asked whether PIP_2 interacts with the S6Jx domain in

Table 1

Effects of mutations on the properties and PIP_2 apparent affinities of KCNQ3 channels

Values represent mean ± S.E. *, **, and ***, $p < 0.05$, $p < 0.01$, and $p < 0.001$ (one-way analysis of variance with Dunnett's multiple-comparison test) statistically different from WT. ND, not determined.

		Channel function		Rates from Dr-VSP assays		
KCNQ3T	Structural domain	Current density	$V_{½}$	τ, decay at +120 mV	τ, recovery at +30 mV	M_1R inhibition
		pA/pF	*mV*	*s*	*s*	*%*
WT		197 ± 6 (n = 19)	−34.0 ± 1.9 (n = 19)	0.94 ± 0.13 (n = 10)	7.5 ± 1.7 (n = 11)	29.5 ± 5.5 (n = 3)
R190Q	S2–S3 linker	66 ± 12*** (n = 6)	−39.9 ± 1.9 (n = 5)	0.35 ± 0.11** (n = 8)	9.6 ± 1.6 (n = 8)	63 ± 13 (n = 6)
R195Q	S2–S3 linker	195 ± 13 (n = 6)	−36.0 ± 1.8 (n = 6)	0.98 ± 0.22 (n = 5)	7.4 ± 1.0 (n = 5)	24.9 ± 5.8 (n = 7)
R242A	S4–S5 linker	146 ± 16*** (n = 10)	−4.0 ± 3.2*** (n = 7)	0.77 ± 0.13 (n = 10)	14.2 ± 1.7* (n = 10)	64.8 ± 9.2 (n = 3)
R243A	S4–S5 linker	56 ± 16*** (n = 4)	−31 ± 4.7 (n = 4)	0.59 ± 0.19* (n = 4)	13.1 ± 1.8* (n = 4)	42 ± 5.5 (n = 3)
R242A/R243A	S4–S5 linker	65 ± 11*** (n = 11)	−0.2 ± 2.9*** (n = 5)	0.45 ± 0.11** (n = 5)	15 ± 1.7* (n = 5)	91.6 ± 2.7 (n = 4)
H257N	S4–S5 linker	30 ± 3*** (n = 7)	2.5 ± 2.8*** (n = 7)	0.58 ± 0.14* (n = 4)	11.03 ± 1.4 (n = 2)	81.6 ± 7.9 (n = 4)
K358A	S6Jx	195 ± 7 (n = 9)	−28.8 ± 2.2 (n = 9)	0.94 ± 0.25 (n = 6)	8.0 ± 1.7 (n = 6)	ND
R364A	S6Jx	72 ± 8*** (n = 6)	−30.1 ± 2 (n = 6)	0.14 ± 0.02*** (n = 5)	27.7 ± 6.9*** (n = 5)	ND
K366A	S6Jx	187 ± 12 (n = 8)	−29.6 ± 1.3 (n = 8)	0.95 ± 0.12 (n = 7)	9.2 ± 1.7 (n = 6)	ND
KRK/AAA	S6Jx	79 ± 11*** (n = 8)	−6.3 ± 2.5*** (n = 7)	0.29 ± 0.04*** (n = 7)	17.9 ± 2.6*** (n = 6)	ND
H367C	S6Jx	138 ± 5** (n = 6)	−25.0 ± 2.1* (n = 6)	0.32 ± 0.05** (n = 6)	36.7 ± 6.9*** (n = 6)	ND
(Δ linker)	C terminus	112 ± 10*** (n = 11)	−32.5 ± 1.5 (n = 11)	0.26 ± 0.04*** (n = 7)	13.5 ± 2.2* (n = 7)	ND
RH-AC/Δ linker	C terminus	16 ± 2*** (n = 8)	ND	0.53 ± 0.1* (n = 6)	45.8 ± 5.2*** (n = 6)	ND
K531N	C terminus	193 ± 54 (n = 8)	−20.3 ± 6 (n = 4)	1.05 ± 0.33 (n = 7)	10 ± 0.9 (n = 7)	ND
K532N	C terminus	204 ± 48 (n = 8)	−19.9 ± 2.6 (n = 6)	1.01 ± 0.32 (n = 8)	9.08 ± 1.4 (n = 8)	ND
K533N	C terminus	208 ± 62 (n = 7)	−21.1 ± 3.4 (n = 7)	0.86 ± 0.12 (n = 8)	8.62 ± 0.6 (n = 8)	ND

KCNQ3T channels (Fig. 3). We found that the R364A mutation significantly decreased current amplitudes (72 ± 8 pA/pF *versus* 197 ± 6 pA/pF for KCNQ3T), whereas the K358A and K366A mutations did not (195 ± 7 and 187 ± 12 pA/pF, respectively) (Fig. 3, *A* and *B*). As before, we measured the responses of each mutant to PIP_2 dephosphorylation by Dr-VSP and the rate of recovery upon Dr-VSP turn-off and found the R364A mutation to result in a much faster decay of the current (0.14 ± 0.02 s) upon activation of Dr-VSP and a much slower recovery of the current (27.7 ± 6.9 s) upon its turn off (Fig. 3 (*D–F*), Fig. S1 (*C* and *D*), and Table 1). Neither response was altered for K358A and K366A (Fig. 3 (*D–F*) and Table 1); nor was the maximal inhibition by M_1R stimulation (25.1 ± 6.8%).

We also tested the effect of the K358A and K366A mutations in combination with R364A as the triple mutant KRK/AAA. The KRK/AAA mutant decreased the current amplitude similarly to that of R364A (79 ± 11 pA/pF), and such channels displayed a similarly reduced apparent affinity for PIP_2 (τ_{decay} = 0.29 ± 0.04 s and $\tau_{recovery}$ = 17.9 ± 2.6 s, n = 6–7, $p < 0.001$) using the Dr-VSP assay (Fig. 3 (*A*, *B*, and *D–F*) and Table 1), echoing the results of the single point mutants. None of these single point mutations significantly affected channel voltage dependence (Fig. 3*C*). Strikingly, however, the KRK/AAA triple mutation uniquely in this domain resulted in channels with a voltage dependence of activation markedly shifted toward more positive potentials. For KCNQ3T and KCNQ3T-KRK/AAA, the half-activation potentials were −34.0 ± 1.9 and −6.3 ± 2.5 mV, respectively. We also tested the effects of the H367C mutation on KCNQ3T, which is slightly downstream of Arg^{364} in the S6Jx domain. This mutation only slightly reduced current densities (138 ± 5 pA/pF) but significantly increased the rate of decay of the current (0.32 ± 0.05 s) upon activation of Dr-VSP and slowed its recovery (36.7 ± 6.9 s) upon Dr-VSP turn-off, indicating an interaction of this residue with PIP_2, as shown for KCNQ2 (4). Such mutant channels displayed no significant shift in the voltage dependence of activation (Fig. 3*C* and Table 1). Taken together, these results strongly implicate the S6Jx domain of KCNQ3 channels as an important site for PIP_2 interactions, as for KCNQ1 channels, and this altered apparent affinity for PIP_2 also seems not linked to an altered voltage dependence of activation.

The A–B helix linker contributes strongly to the apparent affinity for PIP_2

We previously identified a cluster of basic residues (Lys^{425}, Lys^{432}, and Arg^{434}) within the linker between helices A and B (A–B linker) of both KCNQ2 and KCNQ3 to be critical for PIP_2-mediated control of gating, with the effect of mutations of this cluster in KCNQ2 somewhat more potent than in KCNQ3 (8). However, a study that deleted the A–B helix domain of KCNQ2 did not find that this deleted domain reduced the PIP_2 apparent affinity for KCNQ2 channels (29). Thus, we tested the importance of this domain of KCNQ3 using the same assays as before. We found that the deletion of the A–B linker (Δ linker) decreased whole-cell current amplitudes by about half (112 ± 10 pA/pF; Fig. 4, *A* and *B*). In cells co-expressing KCNQ3T (Δ linker) with Dr-VSP (Fig. 4*D*), the rate of current decay upon Dr-VSP turn-on was ~3-fold faster (0.26 ± 0.04 s), compared with KCNQ3T (Fig. 4*E* and Table 1), and the rate of current recovery upon turn-off of Dr-VSP was significantly slower (13.5 ± 2.2 s) (Fig. 4*F* and Table 1). Such data reinforce a critical role of the helix A–B linker in PIP_2 interactions with KCNQ3 channels, correlating with changes in open probability found for the triple (K425E/K432E/R434E) KCNQ3 mutant within the A–B linker previously studied in excised single-channel patches (8). Lastly, as for the other PIP_2-interacting domains, the KCNQ3T (Δ linker) did not display a significant shift in channel voltage dependence, with $V_{½}$ values for KCNQ3T and KCNQ3T (Δ linker) currents of −34.0 ± 1.9 and −32.5 ± 1.5 mV, respectively (Fig. 4*C* and Table 1).

We wondered what the result would be of combining the RH-AC mutation within the S6Jx domain with the KCNQ3T (Δ linker) mutant. To our surprise, such severely mutated channels nonetheless still yielded very small, but observable, PIP_2-dependent currents (Fig. 4). Thus, the whole-cell current den-

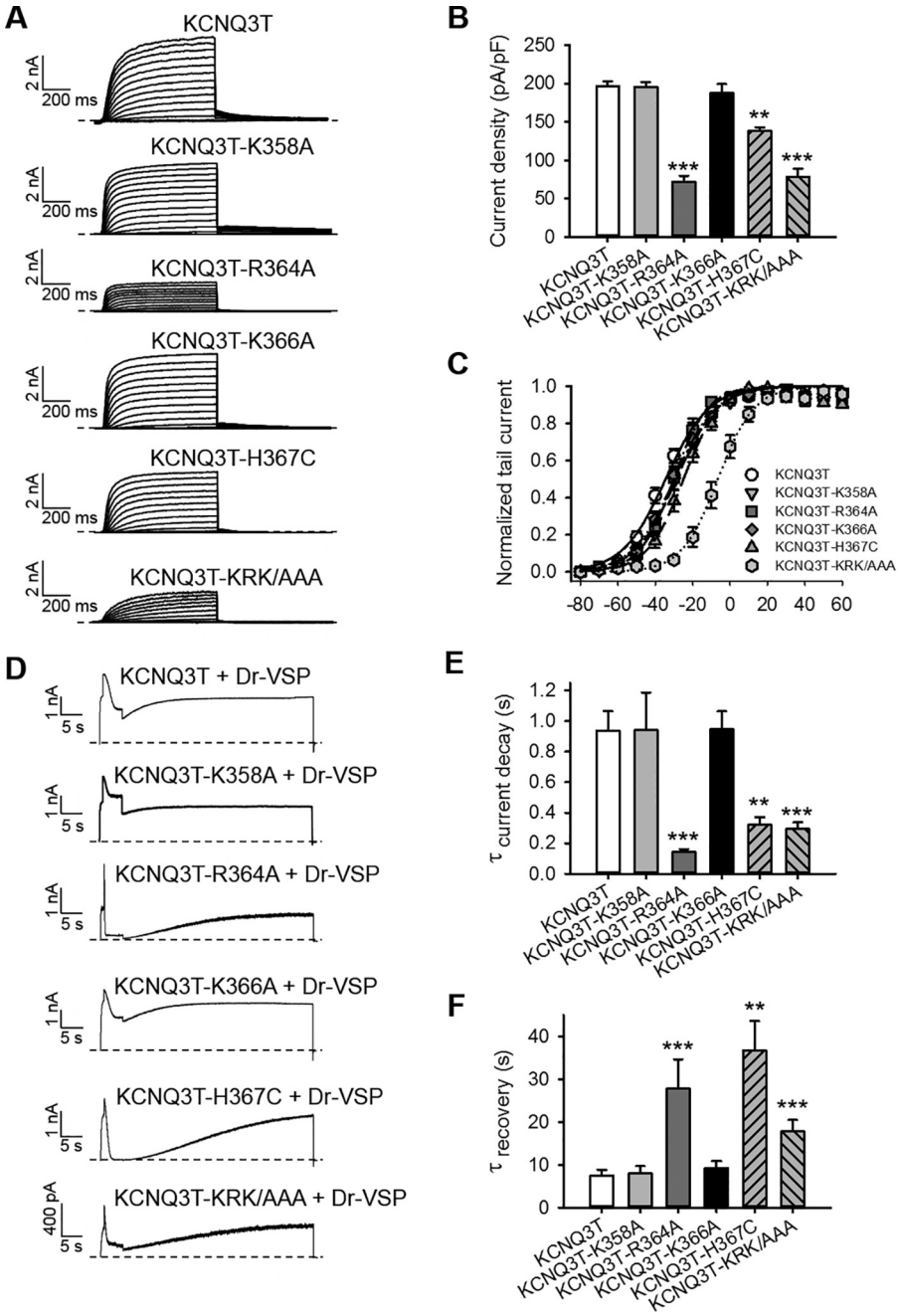

Figure 3. Effects of charge neutralizing mutations located in the S6Jx domain on KCNQ3T channels. *A*, representative perforated patch-clamp recordings from KCNQ3T and mutant channels. *B*, bars show summarized current densities at 60 mV for the indicated channels ($n = 6–19$). *C*, voltage dependence of activation of the tail currents at −60 mV, plotted as a function of test potential ($n = 6–19$). *D*, representative perforated patch-clamp recordings from CHO cells co-transfected with Dr-VSP and KCNQ3T or mutant KCNQ3T channels. *E*, bars summarize time constants from single-exponential fits to current decay during Dr-VSP activation ($n = 5–10$). *F*, bars summarize time constants from single-exponential fits to recovery after Dr-VSP turn-off ($n = 5–11$). The current traces from KCNQ3T in *A* and *D* are from the same cell as in Fig. 2 (*A* and *D*), and the summarized data for KCNQ3T in *B–F* are the same as in Fig. 2, as these data serve as the baseline for all of the sets of mutants shown in Figs. 2–4. KCNQ3T and all mutants were tested contemporaneously. **, $p < 0.01$; ***, $p < 0.001$. *Error bars*, S.E.

sity was dramatically decreased, from 197 ± 6 to 16 ± 2 pA/pF (Fig. 4*B* and Table 1). PIP_2 depletion induced by Dr-VSP rapidly and nearly completely abolished currents from the RH-AC/Δ linker mutant, with a much faster rate of decay upon Dr-VSP turn-on (0.53 ± 0.1 s), and a much slower rate of recovery upon turn-off of Dr-VSP (45.8 ± 5.2 s), than for KCNQ3T channels (Fig. 4 (*D–F*) and Table 1). The small amplitude of the currents from such severely mutated channels tested here precludes any significant meaning from comparing data from those channels and those from the RH-AC or the Δ linker mutant alone. They do reinforce the presence of two major PIP_2-interaction sites within the C terminus of KCNQ3 channels, one in the A–B linker, as previously reported (8), and the other within the S6Jx domain.

Recently, the first two residues of a three-lysine cluster located at the end of the B-helix of KCNQ1 (Lys^{526}-Lys^{527}-Lys^{528}) have been identified as a critical site where CaM competes with PIP_2 to stabilize the open state of KCNQ1-contain-

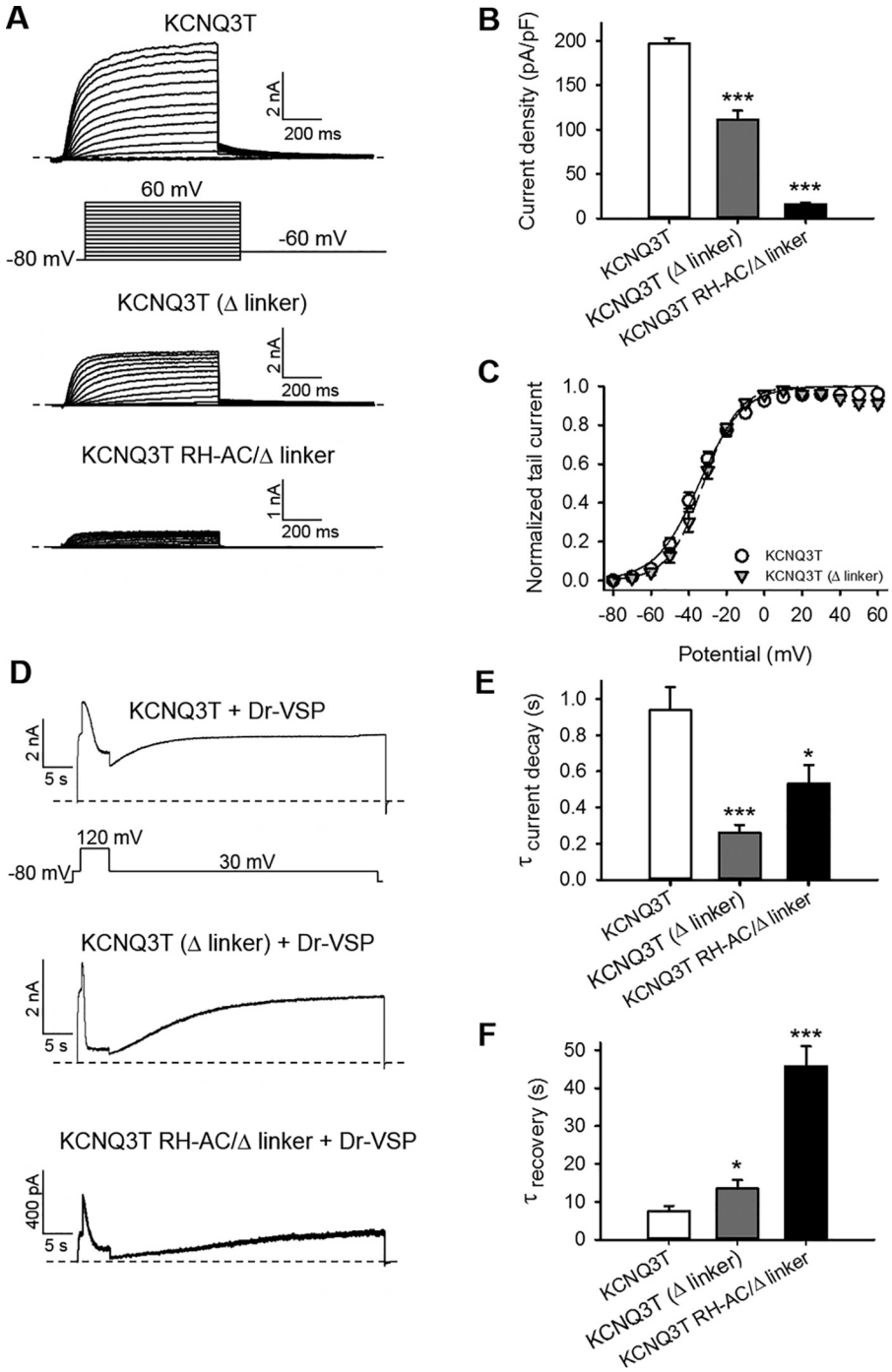

Figure 4. Effects of the A–B linker deletion on KCNQ3T channels. *A*, representative perforated patch-clamp recordings from cells expressing Dr-VSP and either KCNQ3T, KCNQ3T (Δ linker), or KCNQ3T (RH-AC/Δ linker) channels. Cells were held at −80 mV, and voltage steps were applied from −80 to 60 mV in 10-mV increments every 3 s. *B*, bars show summarized current densities at 60 mV for the indicated channels ($n = 8–19$). *C*, shown are the amplitude of tail currents at −60 mV, plotted as a function of test potential from KCNQ3T and KCNQ3T (Δ linker) channels ($n = 11–19$). *D*, representative perforated patch-clamp recordings from CHO cells co-transfected with Dr-VSP and KCNQ3T or KCNQ3T (Δ linker) or the RH-AC/Δ linker mutants. *E*, bars summarize time constants from single-exponential fits to current decay during Dr-VSP activation ($n = 6–10$). *F*, bars summarize time constants from single-exponential fits to recovery after Dr-VSP turn-off ($n = 6–11$). The current traces from KCNQ3T in *A* and *D* are from the same cell as in Fig. 2, *A* and *D*, and the summarized data for KCNQ3T in *B–F* are the same as in Fig. 2, as these data serve as the baseline for all of the sets of mutants shown in Figs. 2–4. KCNQ3T and all mutants were tested contemporaneously. *, $p < 0.05$; ***, $p < 0.001$. *Error bars*, S.E.

ing channels (30, 31). Because this site is conserved in KCNQ3 (Lys^{531}-Lys^{532}-Lys^{533}), we independently mutated the three lysines to asparagines and tested them for interaction with PIP_2 using our VSP approach. Neither the current decay nor recovery was altered for any of the three mutations (Table 1), indicating that this basic cluster is not involved in PIP_2 interactions with KCNQ3. Whether this site plays a role in CaM modulation of KCNQ3 channels remains to be determined. It is likely that the involvement of this domain differs between KCNQ1 and KCNQ3.

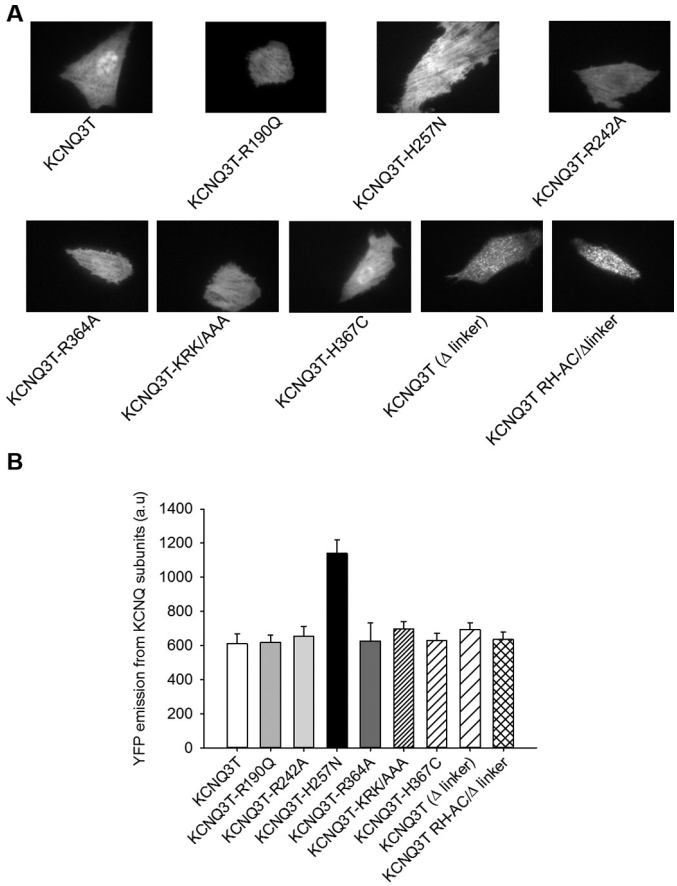

Figure 5. TIRF microscopy indicates that mutants in PIP_2-interacting domains result in minor differences in membrane expression of channels. *A*, fluorescent images under TIRF illumination of CHO cells expressing the indicated enhanced YFP–tagged channels. *B*, *bars* show summarized emission intensity data for each channel type (n = 32–60). *Error bars*, S.E.

Differences in plasma membrane expression of KCNQ3T mutant channels do not explain altered current amplitudes

Because we use whole-cell current amplitudes as one measure of PIP_2 sensitivity in this study, it was incumbent upon us that we rule out the possibility of differential membrane expression of the mutants suggested to have altered apparent affinity for PIP_2, because this would confound our results. We and others have found visualization of membrane proteins tagged with fluorescent proteins under total internal reflection fluorescence (TIRF, evanescent wave) microscopy, which isolates emission from fluorophores within 300 nm of the membrane (32), to be by far the most reliable measure of such membrane expression (20, 33). Under TIRF illumination, we measured the emission from enhanced yellow fluorescent protein (EYFP)-tagged WT and mutant KCNQ3T channels expressed in Chinese hamster ovary (CHO) cells (Fig. 5). These data indicate that the decrease of the whole-cell current density is not due to divergent expression of mutant KCNQ3T channels in the plasma membrane. In fact, the EYFP emission from KCNQ3T + H257N was even higher than that of KCNQ3T, suggesting that the H257N mutation increases the number of channels at the plasma membrane. Thus, differential membrane abundance of channel proteins does not underlie the differences in macroscopic current amplitudes reported in this study.

PIP_2 is predicted to interact with the S4–S5 linker/S6Jx interface of KCNQ3 channels

Our electrophysiological data are consistent with localization of KCNQ3–PIP_2 interactions to four distinct cytoplasmic locations: the A–B helix linker, the S6Jx domain, the S2–S3 linker, and the S4–S5 linker (Fig. S3*E*). In an attempt to construct a framework of these four sites into a coherent structural model of PIP_2 interactions with the channels, we performed homology modeling and PIP_2 docking simulations for all of the mutants studied in this work. Our overall hypothesis emerging from the experimental data supposes a network of interactions between basic residues located in the S2–S3 linker, the S4–S5 linker, and the S6Jx that, together with the A–B helix linker, governs PIP_2-mediated regulation of KCNQ3 channel gating. As above, we divide the channel into three basic modules: the voltage sensor domain (VSD), comprising S2–S4, the pore domain (PD), from S5 to S6, and the C terminus, of which the proximal half (up to the end of the B helix) is the site of several regulatory molecules, and so we call it the regulatory domain. We show models of the VSD, PD, and S6Jx based on the coordinates of the Kv1.2 channel solved in the activated/open conformation (34). Arg^{190} and Arg^{195} lie within the S2–S3 linker, which is part of the VSD; Arg^{242} and His^{257} lie within the PD; and Lys^{358} and Arg^{364} are within the S6Jx, which our model predicts also to be in continuous interface with the PD (Fig. 1 (*B* and *C*); Lys^{366} and His^{367} are not displayed). We did not construct a model of PIP_2 binding to the A–B helix linker, due to the lack of a suitable template.

To model the putative network of interactions of PIP_2 with KCNQ3 channels, we first built structural models of WT and mutant KCNQ3 channels and performed PIP_2 docking simulations to the most energetically favorable WT (Fig. 1, *D* and *E*) and mutant KCNQ3 models (Fig. 6). It is widely thought that positively charged amino acids are mostly responsible for interactions with PIP_2. Thus, we first simulated the interaction of PIP_2 in the presence of all available positive charges on the protein in the open conformation of WT KCNQ3. In the preferred location for PIP_2 binding in the WT KCNQ3 model (Fig. 1*E*), the phosphate headgroup of PIP_2 is predicted to be directed toward Arg^{242} and Arg^{243} in the S4–S5 linker and Lys^{358} and Lys^{366} in the S6Jx and also predicted to form hydrogen-bond interactions with the nearby residues within the same subunit in both the S4–S5 linker and S6Jx (Fig. 1*E*, residues in *blue* in Sub-D). Of note, the acyl tail of PIP_2 is predicted to be directed toward residues in the inner face of S5 (His^{257}) and S6 (Phe^{343}, Phe^{344}, Leu^{346}, and Pro^{347}) in the neighboring subunit (Fig. 1*E*, residues in *orange* in Sub-C). Thus, PIP_2 appears to be cross-linking neighboring subunits, in analogy with a role for PIP_2 reported for GIRK2 channels (35). Taken together, our simulations find that PIP_2 is predicted to interact with the S4–S5 linker/S6Jx interface (Fig. 1*E*), suggesting a mechanistic basis for the effect of mutations in these regions on the favorability for activation (*i.e.* PIP_2 interactions with the S4–S5 linker/S6Jx interface to stabilize and promote opening).

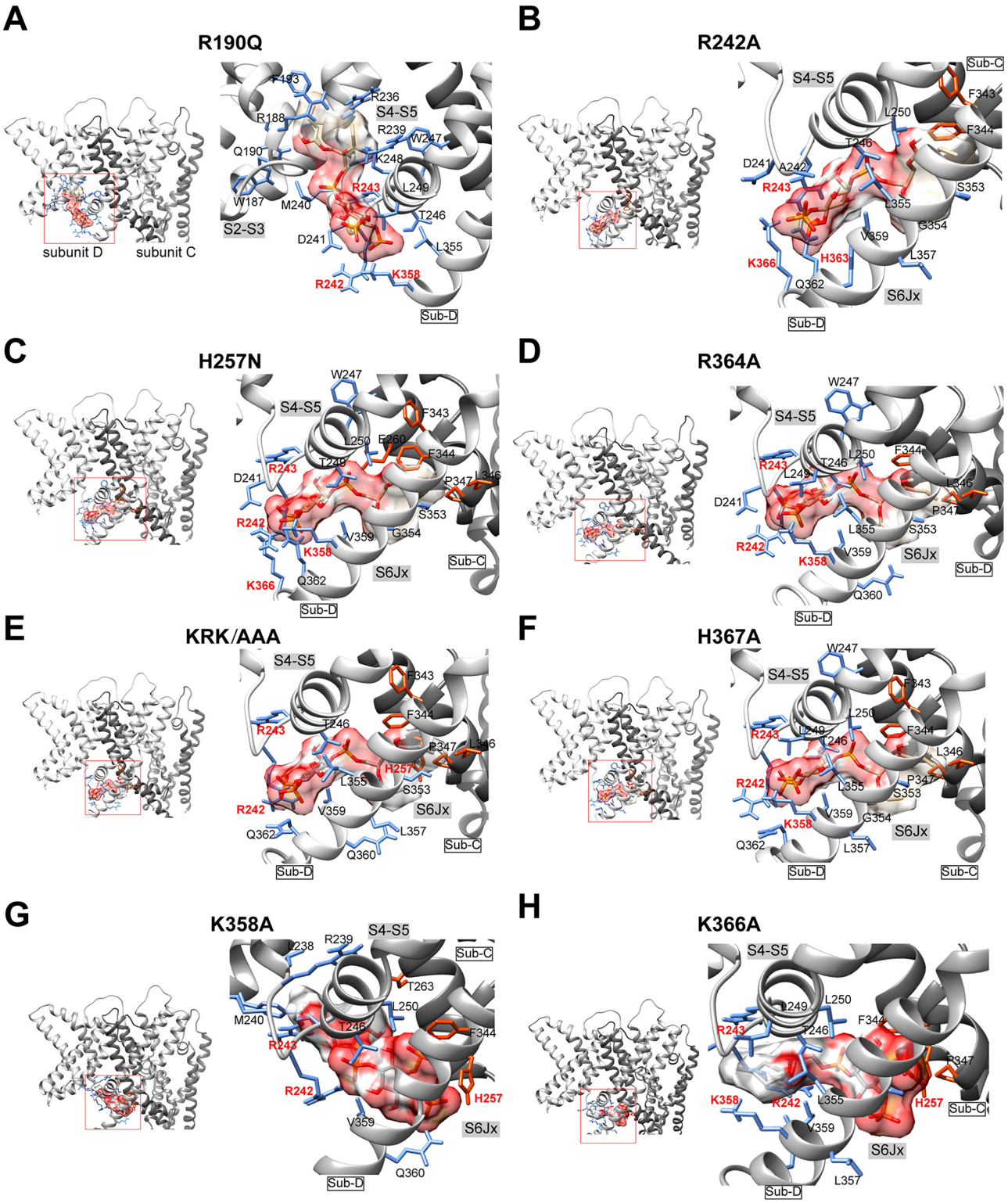

Figure 6. Charge-neutralizing mutations at the S2–S3 and S4–S5 linkers and S6Jx are predicted to disrupt PIP_2 interactions of KCNQ3 channels. Shown are three-dimensional structural models of the most favorable docking PIP_2-docking conformation of the KCNQ3 channel after simulation of charge neutralization at the putative PIP_2-binding site residues Arg^{190} in the S2–S3 linker (*A*); Arg^{242} and His^{257} in the S4–S5 linker (*B* and *C*); and Arg^{364}, Lys^{358}-Arg^{364}-Lys^{366} (KRK/AAA), and His^{367} within the S6Jx (*D–F*). As indicated in Fig. 1, binding sites are enclosed in *red boxes* and enlarged for clarity in the *right panels*. The *top panels* show two neighboring subunits (Sub-C and Sub-D) or a single subunit forming the binding site. The following are the favorable interactions (*labeled* in *red*) predicted to be in the PIP_2-docking network (<6.0 Å, kJ/mol): R190A in *A*, $Arg^{242} = -4.80$, $Arg^{243} = -2.40$, $Lys^{358} = -4.31$; R242A in *B*, $Arg^{243} = -24.9$, $His^{363} = -4.07$, $Lys^{366} = -7.63$; H257N in *C*, $Arg^{242} = -18.8$, $Arg^{243} = -5.41$, $Lys^{358} = -3.11$, $Lys^{366} = -7.52$; R364A in *D*, $Arg^{242} = -12.80$, $Arg^{243} = -4.54$, $Lys^{358} = -3.20$; KRK/AAA in *E*, $Arg^{242} = -27.20$, $Arg^{243} = -3.73$, $His^{257} = -1.23$; H367A in *F*, $Arg^{242} = -10.3$, $Arg^{243} = -3.53$, $Lys^{358} = -5.08$; K358A in *G*, $Arg^{242} = -7.43$, $Arg^{243} = -2.57$, $His^{257} = -5.42$; K366A in *H*, $Arg^{242} = -4.62$, $Arg^{243} = -2.03$, $His^{257} = -4.34$, $Lys^{358} = -2.78$. *Error bars*, S.E.

Multiple sites of PIP_2 interactions at the VSD–PD interface of mutant KCNQ3 channels

In line with previous studies on KCNQ1 and KCNQ2 channels (11, 28), positively charged residues of the S4–S5 linker (Arg^{242} and Arg^{243}) and S6Jx (Lys^{358} and Lys^{366}) in the same subunit (Fig. 1*E*, residues *colored* in *blue*) and S5 of the neighboring subunit (His^{257}) (Fig. 1*E*, residues *colored* in *orange*) are predicted to be involved in the interactions of PIP_2 with WT KCNQ3. However, our experimental data demonstrate that mainly Arg^{190}, Arg^{242}, Arg^{243}, His^{257}, Arg^{364}, and His^{367} are the determinants of PIP_2 interactions, whereas Lys^{358} and Lys^{366} did not seem important. Therefore, we used our model to ask whether these sites are predicted to alter PIP_2 interactions. We analyzed PIP_2 docking simulations for the following mutants: R190Q, R242A, H257N, R364A, KRK/AAA, H367A, K358A, and K366A (Fig. 6). Unlike WT KCNQ3, PIP_2 docking simulations of R190Q (Fig. 6*A*), H257N (Fig. 6*C*), R364A (Fig. 6*D*), H367A (Fig. 6*F*), and K366A (Fig. 6*H*) predict a network of interactions mainly with two positively charged residues of the S4–S5 linker (Arg^{242} and Arg^{243}) and one in S6Jx (Lys^{358}) of the same subunit. Simulations of KRK/AAA (Fig. 6*E*) and K358A (Fig. 6*G*) mutants predict that PIP_2 interacts similarly with Arg^{242} and Arg^{243} of the S4–S5 linker but in those cases stabilizes the network of interactions with His^{257} in S5 of the neighboring subunit. Noteworthy for all these mutants, Arg^{242} is predicted as a common residue in the network of interactions of PIP_2. Moreover, PIP_2 docking simulations of R242A (Fig. 6*B*) suggest a network of interactions with Arg^{243} of the S4–S5 linker and two positively charged residues in S6Jx (His^{363} and Lys^{366}). Moreover, the R242A, H257N, and KRK/AAA mutations are predicted to cause major structural rearrangements in the S4–S5 linker, S5, S6, and S6Jx (Fig. S2). Again, we realize that the experimental data reported little functional effects of charge neutralization of the Lys^{358} and Lys^{366} residues that might have been predicted to stabilize the interactions of PIP_2 with the channels. However, the simulations of PIP_2 with K358A and K366A (Fig. 6, *G* and *H*) predict that whereas the orientation of PIP_2 in the inner face of S6Jx is opposite of that predicted for WT channels, the predicted interactions at residues Arg^{242} and His^{257} are predicted to preserve coupling to channel gating by maintaining coupling between the S4–S5 linker and the S6Jx. Alternatively, as stated above, our model may not have such single-residue precision that corresponds to a transmembrane ion channel *in situ*.

Additional sites of PIP_2 interactions at the S2–S3 interface with KCNQ3 channels

Given the lack of correlation between PIP_2 interactions and modification of the voltage dependence of activation observed in our data (Fig. S3*E*), we generated additional structural models of KCNQ3 in the closed state using as a template the coordinates of the Kv1.2 channel solved in the resting/closed state (34). For the modeled closed KCNQ3 channels, the inositol ring of PIP_2 is predicted to be oriented toward Lys^{103} in S1, Arg^{188} in the S2–S3 linker, and Arg^{227} and Arg^{230} in S4, whereas the acyl tail of PIP_2 is predicted to form hydrogen bonds with residues in S2 and S4 within the same subunit (Fig. 7, *A*–*C*). To correlate these predictions with function, we performed additional patch-clamp experiments, evaluating the effect of charge-neutralizing mutations on current density and on the apparent PIP_2 affinity, again using the Dr-VSP approach. We found that substitution of positively charged residues with an alanine significantly reduced the current density of K103A (19.9 ± 2.7 pA/pF) and R188A (20.3 ± 6.5 pA/pF), compared with KCNQ3T (36.5 ± 2.7 pA/pF) but had no effect on R227A and R230A (Table 2). However, all of the mutants displayed an accelerated rate of decay of the current upon turn-on of Dr-VSP, compared with KCNQ3T. For KCNQ3T, KCNQ3T-K103A, KCNQ3T-R188A, KCNQ3T-R227A, and KCNQ3T-R230A, the rates of decay were 0.84 ± 0.13, 0.29 ± 0.05, 0.48 ± 0.11, 0.18 ± 0.03, and 0.20 ± 0.03 s, respectively (Fig. 7*D*). All of the point mutants displayed a slower rate of recovery compared with KCNQ3T. We then wondered whether the combined K103A/R188A or R227A/R230A double mutations would result in a synergistically greater reduction in current density and in apparent PIP_2 affinity than either mutation alone. We found the current density of KCNQ3T-K103A/R188A (21.5 ± 2.9 pA/pF) to be similar to that of the single-point mutations, but the rate of current decay upon turn-on of Dr-VSP was 2-fold faster (0.39 ± 0.05 s) than that of KCNQ3T channels and intermediate between the K103A (0.29 ± 0.05 s) and R188A (0.48 ± 0.11 s) mutants. In contrast, the current density of the R227A/R230A double mutant was significantly lower (23 ± 3 pA/pF) than that of KCNQ3T. Moreover, the rate of current decay upon turn-on of the DR-VSP was 3-fold faster (0.27 ± 0.04 s) than that of KCNQ3T but slower than those from single R227A and R230A mutants (Table 2). Finally, both double mutants displayed a slower current recovery after turn-off of Dr-VSP (25.4 ± 3.4 and 28.6 ± 5.0 s) than KCNQ3T, quite similar to those of single mutants (Table 2). These data suggest that Lys^{103} in S1, Arg^{188} in the S2–S3 linker, and Arg^{227} and Arg^{230} in S4 play roles in PIP_2 interactions with KCNQ3, but that they do not act synergistically. These data are also consistent with the predictions of our modeling/docking simulations, giving us further confidence in the fidelity of our modeling. Interestingly, Arg^{188} is conserved in KCNQ2 but not in other KCNQ channels, suggesting that this residue may also interact with PIP_2 in KCNQ2. Unlike Arg^{188}, Arg^{227} is conserved in all KCNQ channels and may also be involved in PIP_2 interactions with KCNQ1–5 channels.

While this manuscript was being prepared, the structure of most of the frog *Xenopus* oocyte analog of mammalian KCNQ channels, ("KCNQXem") bound to CaM (PDB entry 5VMS) was solved by cryo-EM (36). We here used as a template the mammalian shaker Kv1.2 K^+ channel (37), which has well-validated data to build new structural models based on the highly conserved structural organization of the voltage sensor domain and the pore domain and moreover is not bound by CaM (37–40). Sun and MacKinnon (36) suggested their KCNQXem–CaM complex to be in a "decoupled" state (PIP_2-free state) or in a transitory conformational state between an open PIP_2-bound activated state and a closed PIP_2-bound deactivated state. We analyzed the alignments between Kv1.2 and KCNQXem–CaM structures, along with our KCNQ3 structural model, and found striking differences between the structures that suggested that

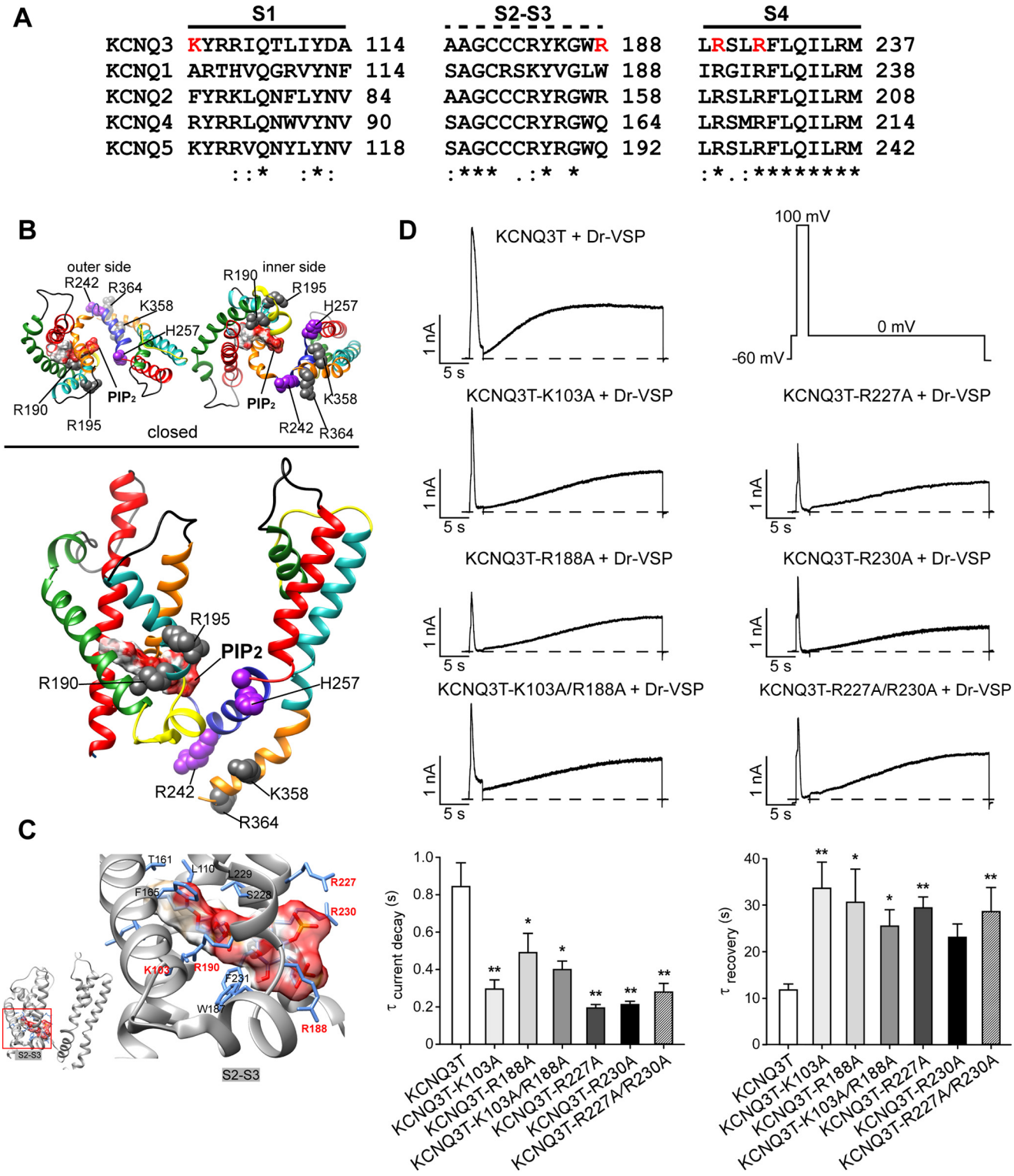

Figure 7. Effects of charge neutralization of residues predicted within the PIP_2 docking site of KCNQ3 in the closed state. *A*, sequence alignments of human KCNQ channels show the additional basic residues Lys^{103}, Arg^{188}, Arg^{227}, and Arg^{230} tested in this study by mutagenesis. The predicted secondary structure of the channel is indicated *above* the alignments as *solid lines* (α-helices) and *noncontinuous lines* (linkers). *B*, *ribbon representations* of the arrangement of the VSD–PD interface of a structural subunit model viewed from the outer and inner side (*upper panels*) and membrane plane (*bottom panels*). The secondary structures of the channels and PIP_2 molecules are shown as in Fig. 1. *C*, expanded view of the most favorable interaction predicted of PIP_2 in the closed-channel state. The phosphate group of the PIP_2 is oriented toward the S2–S3 linker, whereas the acyl tail is enclosed within the α-helices. The following are the favorable interactions (*labeled* in *red*) predicted to be in the PIP_2-docking network (<6.0 Å): $Lys^{103} = -4.03$, $Arg^{188} = -1.44$, $Arg^{190} = -1.52$, $Arg^{227} = -3.23$, $Arg^{230} = -5.36$. *D*, *top*, representative perforated patch-clamp recordings from CHO cells co-transfected with Dr-VSP and KCNQ3T or the indicated mutants. Cells were held at −60 mV, current decay was measured at 100 mV, and recovery of the current was measured at 0 mV after the depolarization to 100 mV. Note the larger amplitude of the recovery current in these experiments after turn-off of Dr-VSP, due to the voltage used (0 mV), at which the "leak" current is expected to be minimal, compared with +30 mV. *Bottom*, *bars* summarize the data from these experiments ($n = 5$–11). *, $p < 0.05$; **, $p < 0.01$. *Error bars*, S.E.

Table 2

Effects on PIP_2 apparent affinity of mutations predicted to interact with KCNQ3 channels in the closed state

Values represent mean ± S.E. * and **, $p < 0.05$ and $p < 0.01$ (one-way analysis of variance with Dunnett's multiple-comparison test) statistically different from WT. ND, not determined.

KCNQ3T	Channel function		Rates from Dr-VSP assays	
	Structural domain	Current density at +0 mV	τ, decay at +100 mV	τ, recovery at +0 mV
		pA/pF	*s*	*s*
WT		36.5 ± 2.7 (n = 11)	0.84 ± 0.13 (n = 11)	11.7 ± 1.3 (n = 11)
K103A	S1	19.9 ± 2.7* (n = 7)	0.29 ± 0.05** (n = 7)	33.6 ± 5.5** (n = 7)
R188A	S2–S3 linker	20.3 ± 6.5* (n = 5)	0.48 ± 0.11* (n = 5)	30.5 ± 7.1* (n = 5)
K103A/R188A	S1/S2–S3 linker	21.5 ± 2.9* (n = 9)	0.39 ± 0.05* (n = 11)	25.4 ± 3.4* (n = 11)
R227A	S4–S5 linker	29.4 ± 5.1 (n = 7)	0.18 ± 0.03** (n = 8)	29.4 ± 2.2** (n = 8)
R230A	S4–S5 linker	30.1 ± 3.4 (n = 11)	0.20 ± 0.03** (n = 11)	22.9 ± 2.8 (n = 11)
K227A/R230A	S4–S5 linker	23 ± 3* (n = 7)	0.27 ± 0.05** (n = 8)	28.6 ± 5.0** (n = 8)

the CaM-free Kv1.2-based KCNQ3 model was superior. The details of those structural comparisons are shown in Fig. S3 (*A–D*).

Discussion

In the present work, we investigate the molecular determinants involved in the regulation of KCNQ3 channels by PIP_2. Many studies have investigated the sites of action of PIP_2 on ion channels, including voltage-dependent K^+ channels (K_v). However, the location of these sites remains controversial. For KCNQ2 and KCNQ3 channels, we have previously highlighted critical PIP_2-interaction domains in the A–B helix linker (8). Others have identified the S6Jx domain as important for KCNQ1–3 (10, 18, 41), and our results here are in accord with those reports. Recent work studying KCNQ1-containing channels has illuminated important PIP_2-interaction domains in the S2–S3 and S4–S5 linkers that play a role in coupling to gating (10, 42, 43). This study is in accord with those findings as well for KCNQ3, in terms of there being additional domains of PIP_2 interactions. Another recent study suggested that the voltage dependence of KCNQ2 channels is regulated via PIP_2 interactions with the S2–S3 and S4–S5 linkers (11). We do not find similar results for KCNQ3. Finally, another group recently suggested that deletion of the A–B linker does not affect the apparent affinity of KCNQ2 for PIP_2 (29); however, in retrospect, we wonder if the VSP method is suitably applicable for such low-PIP_2-affinity channels, given the extremely brief "dwell time" that PIP_2 must manifest for them and a correspondingly high k_{off} rate, especially compared with the rate of PIP_2 dephosphorylation by Dr-VSP. Finally, the current work here, studying KCNQ3, is consistent with our earlier studies implicating the importance of the A–B linker domain (8).

Comparison of the regions of KCNQ1–3 channels contributing to PIP_2 interactions

The present work, reporting that Arg^{364} and His^{367} mutations of KCNQ3T, corresponding to R325A and H328C in KCNQ2, are also highly involved in PIP_2 interactions, is in accord with previous work on KCNQ2 (11, 18). For the family of PIP_2-regulated inward rectifier K^+ (K_{ir}) channels, the JxS6 domain of KCNQ channels is analogous to the C-terminal domain just after M2, which has long been identified as a hot spot for PIP_2 interactions by mutagenesis studies (44) and confirmed by the solved crystal structure of PIP_2 bound to GIRK2 channels (35). Remarkably, our simulation studies predict that PIP_2 is stabilized between neighboring subunits in the S6Jx, which is similar to that reported for GIRK2 channels in the analogous domain. Hence, we suppose this structural mechanism to be likely conserved among PIP_2-regulated channels in general. We speculate that the dual A and B helices, both containing calmodulin-binding domains, possessed by KCNQ, but not K_{ir}, channels, endow the A–B linker of KCNQ channels as a more unique site of PIP_2 interactions, for reasons that will likely require more structural studies of these proteins.

Although our results here also show PIP_2 interactions with the S2–S3 and S4–S5 linkers in the VSD of KCNQ3, as for KCNQ1, and that small, yet definite PIP_2-sensitive and voltage-gated currents are still produced by KCNQ3T channels mutated to lack interactions with both domains in the C terminus, we do not find the interactions with the S2–S3 and S4–S5 linkers to be coupled to modifications of voltage dependence of the currents. Because the work on KCNQ1 channels showed that such linkage to PIP_2 was not via alterations in the sensitivity of the voltage sensor but rather due to the efficiency of coupling between the voltage sensor and the gating machinery (10), we hypothesize that the role of PIP_2 interactions in such coupling is probably similar in nature between KCNQ1 and KCNQ3, and likely KCNQ2 as well. Interestingly, a striking difference between KCNQ1-containing channels and KCNQ2-4 is that whereas currents from the latter are depressed by Ca^{2+}/calmodulin, those of the former are enhanced (45–51). Given that both critical PIP_2-interaction domains in the C terminus of KCNQ1–3 channels are very likely to be surrounded by Ca^{2+}/calmodulin, we are very interested to learn the relationship between calmodulin and PIP_2 interactions and voltage-dependent coupling and the perhaps subtle yet important differences that confer opposite effects of Ca^{2+} loading of calmodulin on the function of KCNQ1-containing channels *versus* KCNQ2–4.

The basic residues of both S2–S3 and S4–S5 linkers are highly conserved among KCNQ channels. In our experiments, K103A, R188A, R190Q, R227A, and R230A, but not the R195Q or R195A mutations, in S1, the S2–S3 linker, and S4 induced a decrease of the apparent affinity for PIP_2. Lys^{162} in the S2–S3 linker of KCNQ2 has been implicated in PIP_2-channel interactions in the closed state, supported by molecular dynamics simulations (11). Our PIP_2-docking simulations of KCNQ3 channels also suggest that PIP_2 interacts with S1 (Lys^{103}), the S2–S3 linker (Arg^{188} and Arg^{190}), and S4 (Arg^{227} and Arg^{230}) of closed

KCNQ3 channels. In the simulations of KCNQ3 (R188A and R190Q), PIP_2 was predicted to interact with the S2–S3 linker and to lose intersubunit contacts, which might favor channel deactivation. As opposed to previous observations in Shaker and Kv1.2 channels in which the S2–S3 linker has been suggested to interact with PIP_2 preferentially in the closed state (52, 53), our experimental results suggest that disruption of PIP_2 interactions with the S2–S3 linker hinder opening. The modeling/docking simulations are consistent with the opening of KCNQ3 channels involving PIP_2 interactions at the VSD–PD interface, consistent with PIP_2/KCNQ channel interactions involving a complex network of basic residues along the VSD–PD interface and the C terminus that cooperatively favor opening. They also suggest that a structural mechanism of channel opening involves PIP_2-mediated intersubunit interactions. Interestingly, such PIP_2-channel interactions have also been described in the crystal structures of $K_{ir}2.2$ and GIRK2 ($K_{ir}3.2$) channels, corresponding to the S4–S5 linker, pore domain, and C terminus in KCNQ channels (12, 35). Although we do not here find the involvement of PIP_2 interactions with the S4–S5 linker *per se* to be coupled to voltage dependence of activation, our electrophysiological data and our homology modeling are fully in accord with S4–S5 linker and S6 being critical in the coupling between the VSD and the pore domain, as is generally widely seen for voltage-dependent K^+ channels (10, 38, 54–56).

Because only charge-neutralizing mutations in the S4–S5 linker (R242A and H257N) and the S6Jx (K358A/R364A/K366A), reduced PIP_2 apparent affinity and shifted the voltage dependence of KCNQ3 toward more depolarized potentials, we hypothesize that 1) cooperation between the S4–S5 linker and the S6Jx stabilizes opening of KCNQ3 and 2) PIP_2 likely plays a role in this coupling, a hypothesis consistent with the Kv1.2–2.1 crystal structure in which anionic lipids are bound at the VSD–PD interface of the channel (57). However, one central question remains unclear as to generality among K^+ channels: Does PIP_2 affect the voltage-sensor movement and, by that mechanism, the voltage dependence of K_v channels, or do any effects of PIP_2 on channel voltage dependence generally arise from changes in coupling between the VSD and the PD? In Kv1.2, replacement of an arginine with a glutamine (R322Q) in the S4–S5 linker, which is involved in VSD–PD coupling, affected the channel voltage dependence of activation when PIP_2 was depleted. Moreover, gating current experiments showed that PIP_2 affects the VSD movement of Shaker channels through interactions with the S4–S5 linker (53). However, unlike for Shaker, depletion of PIP_2 does not affect VSD movement of KCNQ1 homomers (10). Different laboratories have come to divergent conclusions about whether PIP_2-dependent modulation of KCNQ1-containing channels shifts the voltage dependence of activation, with one group positing that it does (3, 58) but another group concluding that it does not (10, 59). Our data here are in accord with the latter conclusion for the case of KCNQ3 channels, consistent with the conclusions for KCNQ2/3 heteromers (23–25). The presence or absence of KCNE1 subunits is unlikely to alter such conclusions for KCNQ1, because KCNE1 was shown to have no direct impact on VSD activation or pore opening, but rather to affect VSD–PD coupling (60). Consistent with this, a point mutation (F351A) at the VSD–PD interface had similar effects on KCNQ1 as did inclusion of KCNE1 in the channel. In that work, both KCNE1 and the F351A mutation abolished the "intermediate-open state" of KCNQ1-containing channels, promoting the activated-open states of KCNQ1 by increasing its PIP_2 affinity (59–61), besides the suppression of inactivation (62). We tentatively conclude that PIP_2 does not contribute generally to the voltage dependence of all KCNQ channels, including KCNQ1, as we found for KCNQ3, but is much more likely to be involved in the efficiency of VSD–PD coupling. We suspect, but cannot at this point provide evidence, that the underlying reason is the display of two distinct open states of all KCNQ channels (42, 63), leading to state transitions, and PIP_2 actions on voltage dependence, differing from those of other K_v channels.

Although we now are in accord with four distinct regions of KCNQ1–3 channels interacting with PIP_2, we cannot rule out yet more PIP_2-binding sites. The distal C terminus contains basic residues that are conserved in all KCNQ channels, which may also contribute to PIP_2. Our experiments show that the triplet of lysines (Lys^{531}, Lys^{532}, and Lys^{533}) located at the end of the B-helix of KCNQ3 do not interact with PIP_2. However, Arg^{539} and Arg^{555} located in the distal C terminus of KCNQ1 (within the C-helix) were reported to decrease the affinity of the channel to DiC8-PIP_2 (26), and Lys^{526}, Lys^{527}, and Lys^{528} have been identified as a critical fifth site where CaM competes with PIP_2 to stabilize the open state of KCNQ1-containing channels (30, 31). The possibility of other PIP_2-interacting sites at the end of the regulatory domain is intriguing, given the location of the site of phosphorylation of KCNQ3 channels by protein kinase C (64), because such phosphorylation would add a counteracting negative charge at that locus. This could be a "hot spot" of PIP_2/protein kinase C cross-talk, both of which are affected by stimulation of G_q-coupled receptors. Such a highly intriguing possibility needs to be carefully examined for all KCNQ2–4 channels as well as KCNQ2/3 heteromers that underlie most M-type K^+ currents in the nervous system.

Experimental procedures

Cell culture and transfection

CHO cells were grown in 100-mm tissue culture dishes (Falcon, Franklin Lakes, NJ) in Dulbecco's modified Eagle's medium with 10% heat-inactivated fetal bovine serum plus 0.1% penicillin/streptomycin in a humidified incubator at 37 °C (5% CO_2) and passaged every 4 days. Cells were discarded after ~30 passages. For patch-clamp and TIRF experiments, CHO cells were first passaged onto 35-mm plastic tissue culture dishes and transfected 24 h later with FuGENE HD reagent (Promega), according to the manufacturer's instructions. The next day, cells were plated onto coverglass chips, and experiments were performed over the following 1–2 days.

Perforated patch electrophysiology

Pipettes were pulled from borosilicate glass capillaries (1B150F-4, World Precision Instruments) using a Flaming/Brown micropipette puller P-97 (Sutter Instruments) and had resistances of 2–4 megaohms when filled with internal solution

and measured in standard bath solution. Membrane current was measured with pipette and membrane capacitance cancellation, sampled at 5 ms, and filtered at 500 Hz by means of an EPC9 amplifier and PULSE software (HEKA/Instrutech). In all experiments, the perforated patch method of recording was used with amphotericin B (600 ng/ml) in the pipette (65). Amphotericin was prepared as a stock solution as 60 mg/ml in DMSO. In these experiments, the access resistance was typically 7–10 megaohms 5–10 min after seal formation. Cells were placed in a 500-μl perfusion chamber through which solution flowed at 1–2 ml/min. Inflow to the chamber was by gravity from several reservoirs, selectable by activation of solenoid valves (Warner Scientific). Bath solution exchange was essentially complete by <30 s. Experiments were performed at room temperature.

Currents were studied by holding the membrane potential at −80 mV and applying 800-ms depolarizing pulses from 60 to −80 mV, every 3 s. Basal KCNQ current amplitudes were measured at 60 mV. To estimate voltage dependence, tail current amplitudes were measured ~10–20 ms after the repolarization at −60 mV, normalized, and plotted as a function of test potential. The data were fit with Boltzmann relations of the form, $I/I_{max} = I_{max}/(1 + \exp((V_{½} - V)/k))$, where I_{max} is the maximum tail current, $V_{½}$ is the voltage that produces half-maximal activation of the conductance, and k is the slope factor. Cell populations were compared using a two-tailed t test. To evaluate the apparent affinity of WT and mutant KCNQ3T channels for PIP_2, we used Dr-VSP cDNA cloned into the pIRES-EGFP bicistronic vector, so that transfected cells would express similar copies of Dr-VSP and EGFP. The cells patched were chosen based on their visible EGFP fluorescence as described previously. Current decay was measured at 120 or 100 mV, normalized, and plotted as a function of time. Recovery of the current was quantified at 30 or 0 mV (which is negative to activation of Dr-VSP) after depolarization to 120 or 100 mV. The rate of current recovery was quantified with a single-exponential fit as described previously, which we realize is an approximation due to the confound of the known rate of PI(4)P-5 kinase ($\tau \sim 10$ s at room temperature) (14), and the rate of current decay was quantified ~30 ms after the activation of Dr-VSP at 120 mV with single exponential fits. Finally, the steady-state inhibition of the current by Dr-VSP was quantified by comparing current at 30 mV or 0 mV before and after activation of Dr-VSP. Data are given as the mean ± S.E.

The external Ringer's solution used to record KCNQ currents in CHO cells contained 160 mM NaCl, 5 mM KCl, 2 mM $CaCl_2$, 1 mM $MgCl_2$, and 10 mM HEPES, pH 7.4, with NaOH. The pipette solution contained 160 mM KCl, 5 mM $MgCl_2$, and 10 mM HEPES, pH 7.4, with KOH, with added amphotericin B (600 ng/ml).

TIRF microscopy

Fluorescence emission from EYFP–tagged KCNQ3T and KCNQ3T mutants (R190Q, R242A, H257N, R364A, KRK/AAA, H367C, Δ linker, and RH-AC/Δ linker) were collected at room temperature using TIRF (also called evanescent field) microscopy. Total internal reflection fluorescence generates evanescent field illumination normal to the interface between two media of differing refractive indices, the coverglass and water in this case, that declines exponentially with distance, illuminating only a thin section (300 nm) of the cell very near the coverglass, including the plasma membrane (32). All TIRF experiments were performed on a Nikon TE2000 microscope mated to a Prairie Technologies laser launch delivery system, as described previously (20). Images were not binned or filtered, with a pixel size corresponding to a square of 122 × 122 nm. The reader should know that this system has now been very significantly upgraded.

Structural homology, simulation, and docking models

The human KCNQ3 channel sequence in FASTA format (Uniprot ID O43525) was loaded into Swiss-PdbViewer version 4.10 (66) for template searching against the ExPDB database (ExPASy). Then the structural model for the full length of the *Rattus norvegicus* voltage-gated K^+ channel subfamily A member 2 (Kv1.2; PDB entry 3LUT) (54) was identified as the best template. The initial sequence alignments between the KCNQ3 channel and Kv1.2 were generated with full-length pairwise alignments using ClustalW (67). Sequence alignments were inspected manually to assure accuracy among structural domains solved from the template. Because the turret domain of the KCNQ3 subunit was absent in the solved Kv1.2 structure, residues 287–296 were excluded from the modeling. The A315T pore mutation was also omitted from the template, because it does not change the apparent PIP_2 affinity of the channel (19). Full-length multiple alignments were submitted for automated comparative protein modeling implemented in the program suite incorporated in SWISS-MODEL (http://swissmodel.expasy.org).[5]

Before energy minimization using GROMOS96 (68), the resulting structural models of KCNQ3 subunits were manually inspected, the structural alignments were confirmed and evaluated for proper hydrogen bonds, and the presence of clashes and missing atoms was estimated using Molegro Molecular Viewer. Further structural models were generated by rearrangement of four KCNQ3 subunit models as a tetramer. Coordinates of the Kv1.2 channel in the resting/closed and activated/open states (34) were used to model the KCNQ3 channel in both forms. The calculated energies for the corresponding KCNQ3 open and closed stated structural models were highly favorable (−35,580 and −27,656 kJ/mol, respectively). Neighborhood structural conformational changes caused by the introduction of single point mutations of the KCNQ3 structure were simulated using Rosetta version 3.1 (69) and implemented in the program suite incorporated in Rosetta Backrub. As Rosetta 3.1 does not allow cysteine substitutions, we modeled KCNQ3 subunits (WT or mutant) with cysteines exchanged for alanines. Simulations for single point mutations were carried out for dimers, for which identical mutations were presented in neighboring subunits, excluding distal residues of the C terminus (residues 404–557).

Up to 20 of the best-scoring structures were generated at each time by choosing parameters recommended by the appli-

[5] Please note that the JBC is not responsible for the long-term archiving and maintenance of this site or any other third party hosted site.

cation. The root-mean square (r.m.s.) deviation was calculated between the WT structures and superimposed on the simulated mutant structures. For each mutation, the r.m.s. average over 10 low-energy structures was computed, and conformational changes were displayed among neighboring structural domains considered significant for values of r.m.s. > 0.5 Å. PatchDock (70), a molecular docking algorithm based on shape complementarity principles, was used to dock PIP_2 with proposed interacting domains at the interfaces of dimer homology models based upon the Kv1.2 structure. One PIP_2 ligand was simulated docked per subunit, with the structure of PIP_2 used as in the solved PIP_2-bound structure of Kv2.2 (12). PatchDock was implemented using an algorithm applied for protein–small ligand docking with a default clustering of 1.5 Å of the r.m.s. as recommended. Before the simulation, a list of residues for three predicted binding sites for PIP_2 in the docking site was derived, as indicated by functional studies, which included domains within the S2–S3 and S4–S5 linkers and the proximal C terminus. Twenty solutions for the first and the fifth best-scoring simulated mutant were ranked according to the geometric shape complementarity score and the atomic contact energy (-171 and -243 kcal/mol for the open and closed states, respectively) (71) and inspected manually to assure accuracy among representative orientations of bound PIP_2. The energy electrostatic interactions for a given docking pose (ligand–protein complex) were analyzed using the ligand energy inspector implemented through the Molegro Molecular viewer. The short-range electrostatic interactions ($r < 6$ Å) between the PIP_2 and residues in WT or mutant were computed, and the lowest solutions among those with the highest geometric score and the right orientation are represented here. We prepared the modeling figures using Chimera version 1.7 (72).

Author contributions—F. S. C., V. D. R., S. M. B., C. C. H., and M. S. S. designed the experiments. C. C. H. performed the simulations and some experiments. F. S. C., V. D. R., and S. M. B performed experiments. M. S. S., F. S. C., V. D. R., and C. C. H. wrote the manuscript and designed the figures.

Acknowledgments—We gratefully acknowledge the assistance of Pamela Reed, Maryann Hobbs, and Isamar Sanchez in this work. We also thank Crystal Archer for useful discussions.

References

1. Jentsch, T. J. (2000) Neuronal KCNQ potassium channels: physiology and role in disease. *Nat. Rev. Neurosci.* **1,** 21–30 CrossRef Medline
2. Suh, B. C., and Hille, B. (2002) Recovery from muscarinic modulation of M current channels requires phosphatidylinositol 4,5-bisphosphate synthesis. *Neuron* **35,** 507–520 CrossRef Medline
3. Loussouarn, G., Park, K. H., Bellocq, C., Baró, I., Charpentier, F., and Escande, D. (2003) Phosphatidylinositol-4,5-bisphosphate, PIP2, controls KCNQ1/KCNE1 voltage-gated potassium channels: a functional homology between voltage-gated and inward rectifier K^+ channels. *EMBO J.* **22,** 5412–5421 CrossRef Medline
4. Zhang, H., Craciun, L. C., Mirshahi, T., Rohács, T., Lopes, C. M., Jin, T., and Logothetis, D. E. (2003) PIP_2 activates KCNQ channels, and its hydrolysis underlies receptor-mediated inhibition of M currents. *Neuron* **37,** 963–975 CrossRef Medline
5. Li, Y., Gamper, N., Hilgemann, D. W., and Shapiro, M. S. (2005) Regulation of Kv7 (KCNQ) K^+ channel open probability by phosphatidylinositol 4,5-bisphosphate. *J. Neurosci.* **25,** 9825–9835 CrossRef Medline
6. Winks, J. S., Hughes, S., Filippov, A. K., Tatulian, L., Abogadie, F. C., Brown, D. A., and Marsh, S. J. (2005) Relationship between membrane phosphatidylinositol-4,5-bisphosphate and receptor-mediated inhibition of native neuronal M channels. *J. Neurosci.* **25,** 3400–3413 CrossRef Medline
7. Gamper, N., and Shapiro, M. S. (2007) Regulation of ion transport proteins by membrane phosphoinositides. *Nat. Rev. Neurosci.* **8,** 921–934 CrossRef Medline
8. Hernandez, C. C., Zaika, O., and Shapiro, M. S. (2008) A carboxy-terminal inter-helix linker as the site of phosphatidylinositol 4,5-bisphosphate action on Kv7 (M-type) K^+ channels. *J. Gen. Physiol.* **132,** 361–381 CrossRef Medline
9. Thomas, A. M., Harmer, S. C., Khambra, T., and Tinker, A. (2011) Characterization of a binding site for anionic phospholipids on KCNQ1. *J. Biol. Chem.* **286,** 2088–2100 CrossRef Medline
10. Zaydman, M. A., Silva, J. R., Delaloye, K., Li, Y., Liang, H., Larsson, H. P., Shi, J., and Cui, J. (2013) Kv7.1 ion channels require a lipid to couple voltage sensing to pore opening. *Proc. Natl. Acad. Sci. U.S.A.* **110,** 13180–13185 CrossRef Medline
11. Zhang, Q., Zhou, P., Chen, Z., Li, M., Jiang, H., Gao, Z., and Yang, H. (2013) Dynamic PIP_2 interactions with voltage sensor elements contribute to KCNQ2 channel gating. *Proc. Natl. Acad. Sci. U.S.A.* **110,** 20093–20098 CrossRef Medline
12. Hansen, S. B., Tao, X., and MacKinnon, R. (2011) Structural basis of PIP_2 activation of the classical inward rectifier K^+ channel Kir2.2. *Nature* **477,** 495–498 CrossRef Medline
13. Murata, Y., and Okamura, Y. (2007) Depolarization activates the phosphoinositide phosphatase Ci-VSP, as detected in *Xenopus* oocytes coexpressing sensors of PIP_2. *J. Physiol.* **583,** 875–889 CrossRef Medline
14. Falkenburger, B. H., Jensen, J. B., and Hille, B. (2010) Kinetics of PIP_2 metabolism and KCNQ2/3 channel regulation studied with a voltage-sensitive phosphatase in living cells. *J. Gen. Physiol.* **135,** 99–114 CrossRef Medline
15. Kruse, M., Hammond, G. R., and Hille, B. (2012) Regulation of voltage-gated potassium channels by $PI(4,5)P_2$. *J. Gen. Physiol.* **140,** 189–205 CrossRef Medline
16. Itsuki, K., Imai, Y., Okamura, Y., Abe, K., Inoue, R., and Mori, M. X. (2012) Voltage-sensing phosphatase reveals temporal regulation of TRPC3/C6/C7 channels by membrane phosphoinositides. *Channels* **6,** 206–209 CrossRef Medline
17. Telezhkin, V., Reilly, J. M., Thomas, A. M., Tinker, A., and Brown, D. A. (2012) Structural requirements of membrane phospholipids for M-type potassium channel activation and binding. *J. Biol. Chem.* **287,** 10001–10012 CrossRef Medline
18. Telezhkin, V., Thomas, A. M., Harmer, S. C., Tinker, A., and Brown, D. A. (2013) A basic residue in the proximal C-terminus is necessary for efficient activation of the M-channel subunit Kv7.2 by $PI(4,5)P_2$. *Pflugers Arch.* **465,** 945–953 CrossRef Medline
19. Hernandez, C. C., Falkenburger, B., and Shapiro, M. S. (2009) Affinity for phosphatidylinositol 4,5-bisphosphate determines muscarinic agonist sensitivity of Kv7 K^+ channels. *J. Gen. Physiol.* **134,** 437–448 CrossRef Medline
20. Zaika, O., Hernandez, C. C., Bal, M., Tolstykh, G. P., and Shapiro, M. S. (2008) Determinants within the turret and pore-loop domains of KCNQ3 K^+ channels governing functional activity. *Biophys. J.* **95,** 5121–5137 CrossRef Medline
21. Choveau, F. S., Hernandez, C. C., Bierbower, S. M., and Shapiro, M. S. (2012) Pore determinants of KCNQ3 K^+ current expression. *Biophys. J.* **102,** 2489–2498 CrossRef Medline
22. Bender, K., Wellner-Kienitz, M. C., and Pott, L. (2002) Transfection of a phosphatidyl-4-phosphate 5-kinase gene into rat atrial myocytes removes inhibition of GIRK current by endothelin and α-adrenergic agonists. *FEBS Lett.* **529,** 356–360 CrossRef Medline
23. Shapiro, M. S., Roche, J. P., Kaftan, E. J., Cruzblanca, H., Mackie, K., and Hille, B. (2000) Reconstitution of muscarinic modulation of the KCNQ2/

KCNQ3 K^+ channels that underlie the neuronal M current. *J. Neurosci.* **20,** 1710–1721 CrossRef Medline
24. Suh, B. C., Inoue, T., Meyer, T., and Hille, B. (2006) Rapid chemically induced changes of PtdIns(4,5)P_2 gate KCNQ ion channels. *Science* **314,** 1454–1457 CrossRef Medline
25. Nakajo, K., and Kubo, Y. (2005) Protein kinase C shifts the voltage dependence of KCNQ/M channels expressed in *Xenopus* oocytes. *J. Physiol.* **569,** 59–74 CrossRef Medline
26. Park, K. H., Piron, J., Dahimene, S., Mérot, J., Baró, I., Escande, D., and Loussouarn, G. (2005) Impaired KCNQ1-KCNE1 and phosphatidylinositol-4,5-bisphosphate interaction underlies the long QT syndrome. *Circ. Res.* **96,** 730–739 CrossRef Medline
27. Zhou, P., Yu, H., Gu, M., Nan, F. J., Gao, Z., and Li, M. (2013) Phosphatidylinositol 4,5-bisphosphate alters pharmacological selectivity for epilepsy-causing KCNQ potassium channels. *Proc. Natl. Acad. Sci. U.S.A.* **110,** 8726–8731 CrossRef Medline
28. Eckey, K., Wrobel, E., Strutz-Seebohm, N., Pott, L., Schmitt, N., and Seebohm, G. (2014) Novel Kv7.1-phosphatidylinositol 4,5-bisphosphate interaction sites uncovered by charge neutralization scanning. *J. Biol. Chem.* **289,** 22749–22758 CrossRef Medline
29. Aivar, P., Fernández-Orth, J., Gomis-Perez, C., Alberdi, A., Alaimo, A., Rodríguez, M. S., Giraldez, T., Miranda, P., Areso, P., and Villarroel, A. (2012) Surface expression and subunit specific control of steady protein levels by the Kv7.2 helix A-B linker. *PLoS One* **7,** e47263 CrossRef Medline
30. Tobelaim, W. S., Dvir, M., Lebel, G., Cui, M., Buki, T., Peretz, A., Marom, M., Haitin, Y., Logothetis, D. E., Hirsch, J. A., and Attali, B. (2017) Ca^{2+}-calmodulin and PIP_2 interactions at the proximal C-terminus of Kv7 channels. *Channels* **11,** 686–695 CrossRef Medline
31. Tobelaim, W. S., Dvir, M., Lebel, G., Cui, M., Buki, T., Peretz, A., Marom, M., Haitin, Y., Logothetis, D. E., Hirsch, J. A., and Attali, B. (2017) Competition of calcified calmodulin N lobe and PIP_2 to an LQT mutation site in Kv7.1 channel. *Proc. Natl. Acad. Sci. U.S.A.* **114,** E869–E878 CrossRef Medline
32. Axelrod, D. (2003) Total internal reflection fluorescence microscopy in cell biology. *Methods Enzymol.* **361,** 1–33 CrossRef Medline
33. Boyer, S. B., and Slesinger, P. A. (2010) Probing novel GPCR interactions using a combination of FRET and TIRF. *Commun. Integr. Biol.* **3,** 343–346 CrossRef Medline
34. Khalili-Araghi, F., Jogini, V., Yarov-Yarovoy, V., Tajkhorshid, E., Roux, B., and Schulten, K. (2010) Calculation of the gating charge for the Kv1.2 voltage-activated potassium channel. *Biophys. J.* **98,** 2189–2198 CrossRef Medline
35. Whorton, M. R., and MacKinnon, R. (2011) Crystal structure of the mammalian GIRK2 K^+ channel and gating regulation by G proteins, PIP_2, and sodium. *Cell* **147,** 199–208 CrossRef Medline
36. Sun, J., and MacKinnon, R. (2017) Cryo-EM structure of a KCNQ1/CaM complex reveals insights into congenital long-QT syndrome. *Cell* **169,** 1042–1050.e9 CrossRef Medline
37. Long, S. B., Campbell, E. B., and Mackinnon, R. (2005) Crystal structure of a mammalian voltage-dependent Shaker family K+ channel. *Science* **309,** 897–903 CrossRef Medline
38. Long, S. B., Campbell, E. B., and Mackinnon, R. (2005) Voltage sensor of Kv1.2: structural basis of electromechanical coupling. *Science* **309,** 903–908 CrossRef Medline
39. Tombola, F., Pathak, M. M., and Isacoff, E. Y. (2005) How far will you go to sense voltage? *Neuron* **48,** 719–725 CrossRef Medline
40. Yarov-Yarovoy, V., Baker, D., and Catterall, W. A. (2006) Voltage sensor conformations in the open and closed states in ROSETTA structural models of K^+ channels. *Proc. Natl. Acad. Sci. U.S.A.* **103,** 7292–7297 CrossRef Medline
41. Peroz, D., Rodriguez, N., Choveau, F., Baró, I., Mérot, J., and Loussouarn, G. (2008) Kv7.1 (KCNQ1) properties and channelopathies. *J. Physiol.* **586,** 1785–1789 CrossRef Medline
42. Zaydman, M. A., and Cui, J. (2014) PIP_2 regulation of KCNQ channels: biophysical and molecular mechanisms for lipid modulation of voltage-dependent gating. *Front. Physiol.* **5,** 195 Medline
43. Kasimova, M. A., Zaydman, M. A., Cui, J., and Tarek, M. (2015) PIP_2-dependent coupling is prominent in Kv7.1 due to weakened interactions between S4-S5 and S6. *Sci. Rep.* **5,** 7474 CrossRef Medline
44. Logothetis, D. E., Jin, T., Lupyan, D., and Rosenhouse-Dantsker, A. (2007) Phosphoinositide-mediated gating of inwardly rectifying K^+ channels. *Pflugers Arch.* **455,** 83–95 CrossRef Medline
45. Gamper, N., Li, Y., and Shapiro, M. S. (2005) Structural requirements for differential sensitivity of KCNQ K^+ channels to modulation by Ca^{2+}/calmodulin. *Mol. Biol. Cell* **16,** 3538–3551 CrossRef Medline
46. Gamper, N., and Shapiro, M. S. (2003) Calmodulin mediates Ca^{2+}-dependent modulation of M-type K^+ channels. *J. Gen. Physiol.* **122,** 17–31 CrossRef Medline
47. Chambard, J. M., and Ashmore, J. F. (2005) Regulation of the voltage-gated potassium channel KCNQ4 in the auditory pathway. *Pflugers Arch.* **450,** 34–44 CrossRef Medline
48. Shamgar, L., Ma, L., Schmitt, N., Haitin, Y., Peretz, A., Wiener, R., Hirsch, J., Pongs, O., and Attali, B. (2006) Calmodulin is essential for cardiac IKS channel gating and assembly: impaired function in long-QT mutations. *Circ. Res.* **98,** 1055–1063 CrossRef Medline
49. Zaika, O., Tolstykh, G. P., Jaffe, D. B., and Shapiro, M. S. (2007) Inositol triphosphate-mediated Ca^{2+} signals direct purinergic P2Y receptor regulation of neuronal ion channels. *J. Neurosci.* **27,** 8914–8926 CrossRef Medline
50. Kosenko, A., and Hoshi, N. (2013) A change in configuration of the calmodulin-KCNQ channel complex underlies Ca^{2+}-dependent modulation of KCNQ channel activity. *PLoS One* **8,** e82290 CrossRef Medline
51. Sachyani, D., Dvir, M., Strulovich, R., Tria, G., Tobelaim, W., Peretz, A., Pongs, O., Svergun, D., Attali, B., and Hirsch, J. A. (2014) Structural basis of a Kv7.1 potassium channel gating module: studies of the intracellular c-terminal domain in complex with calmodulin. *Structure* **22,** 1582–1594 CrossRef Medline
52. Abderemane-Ali, F., Es-Salah-Lamoureux, Z., Delemotte, L., Kasimova, M. A., Labro, A. J., Snyders, D. J., Fedida, D., Tarek, M., Baró, I., and Loussouarn, G. (2012) Dual effect of phosphatidylinositol (4,5)-bisphosphate PIP_2 on Shaker K^+ channels. *J. Biol. Chem.* **287,** 36158–36167 CrossRef Medline
53. Rodriguez-Menchaca, A. A., Adney, S. K., Tang, Q. Y., Meng, X. Y., Rosenhouse-Dantsker, A., Cui, M., and Logothetis, D. E. (2012) PIP_2 controls voltage-sensor movement and pore opening of Kv channels through the S4-S5 linker. *Proc. Natl. Acad. Sci. U.S.A.* **109,** E2399–E2408 CrossRef Medline
54. Chen, X., Wang, Q., Ni, F., and Ma, J. (2010) Structure of the full-length Shaker potassium channel Kv1.2 by normal-mode-based X-ray crystallographic refinement. *Proc. Natl. Acad. Sci. U.S.A.* **107,** 11352–11357 CrossRef Medline
55. Choveau, F. S., Rodriguez, N., Abderemane Ali, F., Labro, A. J., Rose, T., Dahimène, S., Boudin, H., Le Hénaff, C., Escande, D., Snyders, D. J., Charpentier, F., Mérot, J., Baró, I., and Loussouarn, G. (2011) KCNQ1 channels voltage dependence through a voltage-dependent binding of the S4-S5 linker to the pore domain. *J. Biol. Chem.* **286,** 707–716 CrossRef Medline
56. Labro, A. J., Boulet, I. R., Choveau, F. S., Mayeur, E., Bruyns, T., Loussouarn, G., Raes, A. L., and Snyders, D. J. (2011) The S4-S5 linker of KCNQ1 channels forms a structural scaffold with the S6 segment controlling gate closure. *J. Biol. Chem.* **286,** 717–725 CrossRef Medline
57. Long, S. B., Tao, X., Campbell, E. B., and MacKinnon, R. (2007) Atomic structure of a voltage-dependent K^+ channel in a lipid membrane-like environment. *Nature* **450,** 376–382 CrossRef Medline
58. Lopes, C. M., Rohács, T., Czirják, G., Balla, T., Enyedi, P., and Logothetis, D. E. (2005) PIP_2 hydrolysis underlies agonist-induced inhibition and regulates voltage gating of two-pore domain K^+ channels. *J. Physiol.* **564,** 117–129 CrossRef Medline
59. Li, Y., Zaydman, M. A., Wu, D., Shi, J., Guan, M., Virgin-Downey, B., and Cui, J. (2011) KCNE1 enhances phosphatidylinositol 4,5-bisphosphate (PIP_2) sensitivity of IKs to modulate channel activity. *Proc. Natl. Acad. Sci. U.S.A.* **108,** 9095–9100 CrossRef Medline
60. Zaydman, M. A., Kasimova, M. A., McFarland, K., Beller, Z., Hou, P., Kinser, H. E., Liang, H., Zhang, G., Shi, J., Tarek, M., and Cui, J. (2014) Domain-domain interactions determine the gating, permeation, pharma-

cology, and subunit modulation of the IKs ion channel. *eLife* **3,** e03606 CrossRef Medline
61. Cui, J. (2016) Voltage-dependent gating: novel insights from KCNQ1 channels. *Biophys. J.* **110,** 14–25 CrossRef Medline
62. Hou, P., Eldstrom, J., Shi, J., Zhong, L., McFarland, K., Gao, Y., Fedida, D., and Cui, J. (2017) Inactivation of KCNQ1 potassium channels reveals dynamic coupling between voltage sensing and pore opening. *Nat. Commun.* **8,** 1730 CrossRef Medline
63. Selyanko, A. A., and Brown, D. A. (1999) M-channel gating and simulation. *Biophys. J.* **77,** 701–713 CrossRef Medline
64. Hoshi, N., Zhang, J. S., Omaki, M., Takeuchi, T., Yokoyama, S., Wanaverbecq, N., Langeberg, L. K., Yoneda, Y., Scott, J. D., Brown, D. A., and Higashida, H. (2003) AKAP150 signaling complex promotes suppression of the M-current by muscarinic agonists. *Nat. Neurosci.* **6,** 564–571 CrossRef Medline
65. Rae, J., Cooper, K., Gates, P., and Watsky, M. (1991) Low access resistance perforated patch recordings using amphotericin B. *J. Neurosci. Methods* **37,** 15–26 CrossRef Medline
66. Schwede, T., Kopp, J., Guex, N., and Peitsch, M. C. (2003) SWISS-MODEL: an automated protein homology-modeling server. *Nucleic Acids Res.* **31,** 3381–3385 CrossRef Medline
67. Thompson, J. D., Higgins, D. G., and Gibson, T. J. (1994) CLUSTAL W: improving the sensitivity of progressive multiple sequence alignment through sequence weighting, position-specific gap penalties and weight matrix choice. *Nucleic Acids Res.* **22,** 4673–4680 CrossRef Medline
68. Schuler, L. D., Daura, X., and Van Gunsteren, W. F. (2001) An improved GROMOS96 force field for aliphatic hydrocarbons in the condensed phase. *J. Comput. Chem.* **22,** 1205–1218 CrossRef
69. Smith, C. A., and Kortemme, T. (2008) Backrub-like backbone simulation recapitulates natural protein conformational variability and improves mutant side-chain prediction. *J. Mol. Biol.* **380,** 742–756 CrossRef Medline
70. Schneidman-Duhovny, D., Inbar, Y., Nussinov, R., and Wolfson, H. J. (2005) PatchDock and SymmDock: servers for rigid and symmetric docking. *Nucleic Acids Res.* **33,** W363–W367 CrossRef Medline
71. Zhang, C., Vasmatzis, G., Cornette, J. L., and DeLisi, C. (1997) Determination of atomic desolvation energies from the structures of crystallized proteins. *J. Mol. Biol.* **267,** 707–726 CrossRef Medline
72. Pettersen, E. F., Goddard, T. D., Huang, C. C., Couch, G. S., Greenblatt, D. M., Meng, E. C., and Ferrin, T. E. (2004) UCSF Chimera: a visualization system for exploratory research and analysis. *J. Comput. Chem.* **25,** 1605–1612 CrossRef Medline
73. Etxeberria, A., Santana-Castro, I., Regalado, M. P., Aivar, P., and Villarroel, A. (2004) Three mechanisms underlie KCNQ2/3 heteromeric potassium M-channel potentiation. *J. Neurosci.* **24,** 9146–9152 CrossRef Medline